TRAF1 controls inflammasome activation by limiting linear ubiquitination of ASC

Safoura Zangiabadi

A THESIS SUBMITTED TO
THE FACULTY OF GRADUATE STUDIES
IN PARTIAL FULFILLMENT OF THE REQUIREMENTS
FOR THE DEGREE OF
MASTER OF SCIENCE

GRADUATE PROGRAM IN KINESIOLOGY AND HEALTH SCIENCE
YORK UNIVERSITY
TORONTO, ONTARIO

April 2021

Abstract

Inflammasomes are multimeric protein complexes that act as a critical component of the innate immune system that control the caspase-1 activation and release of a major pro-inflammatory cytokine IL-1β in response to pathogens and cellular damage. The NLRP3 inflammasome is the most well-characterized inflammasome that consists of the NLRP3 sensor, ASC adaptor protein, and pro-caspase-1. Interestingly, excessive activation of NLRP3 inflammasome has been associated with autoinflammatory and autoimmune diseases such as rheumatoid arthritis, gout, and lupus. Therefore, the NLRP3 inflammasome activation is tightly regulated by linear ubiquitination, a form of post translational modification mediated by linear ubiquitin chain assembly (LUBAC). Moreover, tumor necrosis factor receptor (TNFR) associated factor 1 (TRAF1), a key signalling adaptor protein, has been shown to negatively regulate LUBAC and interfere with linear ubiquitination. Therefore, we explored whether TRAF1 can regulate inflammasome activation and the underlying mechanism. To this end, we knocked down the expression of TRAF1 by RNA interference (shRNA) in the human macrophages cell line (THP-1 cells) and induced NLRP3 inflammasome activation using various stimuli including LPS, nigericin, extracellular ATP, and MSU. The activation of NLRP3 inflammasome, including expression of IL-1β, caspase-1, and ASC were assessed by immunoblotting, ELISA, bioluminescence, and immunoprecipitation. Our findings demonstrated that with reduced TRAF1 levels, there was an increased activation of NLRP3 inflammasome characterized by elevated caspase-1 processing and active IL-1β secretion. Mechanistically, we showed that TRAF1 knockdown cells exhibited increased linear ubiquitination and subsequent oligomerization of ASC. Thereby, TRAF1 limits NLRP3 inflammasome activation by interfering with linear ubiquitination of ASC, which results in reduced caspase-1 activation and IL-1β

secretion. These findings provide insights that might lead to the development of novel therapies that target TRAF1 to improve outcomes of NLRP3 inflammasome-related diseases such as RA.

Acknowledgement

I would first like to thank my supervisor, Dr. Ali Abdul-Sater, for giving me the opportunity to work on this project and pursue my master's degree under his invaluable supervision, guidance and support. Thank you for teaching me how to think critically and allowing me to grow as a research scientist.

I would also like to extend my sincere thanks to my lab mates Fatemah A, Jonathan R, Sunpreet S, Mayoorey M, Amandeep A, and Ali A for their incredible help and support throughout this journey. Furthermore, I would like to express my appreciation to my thesis committee members, Dr. Christopher Perry and Dr. Arthur Cheng, for their valuable time and contributions.

I wish to express my sincere gratitude to my parents Yadollah and Farah for all the sacrifices they have made, and the unconditional love, support, and care they provided for me during the course of my studies. My thanks are also extended to my older siblings Nafiseh and Enayat, and my twin brother Younes for their tremendous encouragement and support.

Last but not least, I would like to express my deepest gratitude to Anis, who always believed in me and supported me with his love and care.

Table of Contents

Abstract ii
Acknowledgement iv
Table of Contents v
List of Figures vii
List of Tables viii
List of Abbreviations ix
Chapter 1: Literature Overview 1
1.1 Pattern Recognition Receptors 1
1.2 Inflammasomes 2
1.3 The NLRP3 Inflammasome 4
1.4 Regulation of Inflammasome 6
1.5 Multifaceted Roles of TRAF1 in Signalling Pathways 8
Chapter 2: Rationale and Objectives 11
2.1 Rationale 11
2.2 Objectives 11
2.3 Hypothesis 12
Chapter 3: Experimental procedures 13
3.1 Cell Culture 13
3.2 Lentiviral Transduction for Generation of TRAF1 Knockdown Cells 13
3.2.1 HEK 293T/17 Transfection 13
3.2.2 THP-1 Transduction 14
3.3 Assessing TRAF1 Expression in shControl and shTRAF1 THP-1 Cells 14
3.3.1 Cellular Treatments 14
3.3.2 Bradford Protein Assay 15
3.4 CRISPR/Cas9-Mediated Gene Knock-in 16
3.4.1 Pre-electroporation 16
3.4.2 RNP Complexing 16
3.4.3 Electroporation 17
3.4.4 Limiting Dilution and Clonal Expansion 18
3.5 CRISPR/Cas9 Genomic Cleavage Detection in the Bulk-edited Population of THP-1 cells 18
3.6 CRISPR/Cas9 HDR-mediated Knock-in Detection in Positive Control Oligos 19
3.6.1 Annealing Designed Control Oligos with Displacement and Flap-probe Oligos 20
3.6.2 Performing Enzymatic Reaction for Testing Positive Control Oligos 20
3.6.3 Testing Clonal Cell Lines for CRISPR/Cas9 HDR-mediated Knock-in 21

3.6.4 Amplification of the Target Site 21
3.6.5 Annealing of PCR Products with Displacement and Flap-probe Oligos 22
3.6.6 Performing Enzymatic Reaction for Testing the Clonal Cell Lines 22
3.7 Detection of Inflammasome Activation 24
3.7.1 Cellular Stimulation 24
3.7.2 Bioluminescent Caspase-1 Activity 24
3.7.3 Enzyme Linked Immunosorbent Assay (ELISA) 25
3.7.4 Detection of IL-1β and Caspase-1 by Western Blot 26
3.8 ASC Oligomerization Assay 26
3.8.1 Western Blot 26
3.9 Immunoprecipitation 28
3.9.1 Linear Ubiquitin Chains and ASC 28
3.10 Statistical Analysis 29
Chapter 4: Results 30
4.1 Knocking Down TRAF1 Expression in THP-1 Cells 30
4.2 Reduced TRAF1 Levels Lead to Increased IL-1β Processing 31
4.3 Reduced TRAF1 Levels Lead to Increased IL-1β Secretion 33
4.4 Reduced TRAF1 Levels Lead to Increased Caspase-1 Activation 35
4.5 Reduced TRAF1 Levels Lead to Increased Caspase-1 Enzymatic Activity 37
4.6 Reduced TRAF1 Levels Lead to Increased ASC oligomerization 39
4.7 Reduced TRAF1 Levels Lead to Increased ASC Linear ubiquitination 41
4.8 Detection of Single Nucleotide Substitutions in TRAF1 Gene 42
4.8.1 Detecting Wild-Type and SNP Control Oligos 42
4.9 Genomic Cleavage of TRAF1 V203A site targeted by sgRNA in THP-1 Cells 45
4.10 Screening for the Desired CRISPR/Cas9- mediated HDR KI V203A 46
4.11 Sequencing Chromatographs for TRAF1 V203A Locus 48
Chapter 5: Discussion 50
Chapter 6: Future Directions 53
Chapter 7: References 54

List of Figures

FIGURE 1. AN OVERVIEW OF TRAF1 MEDIATED REGULATION OF NLRP3 INFLAMMASOME ACTIVATION VIA LUBAC DOWNSTREAM OF TNFR. 10
FIGURE 2. TRAF1 KNOCKDOWN EXPRESSION IN THP-1 CELLS 31
FIGURE 3. IL-1B PROCESSING IN PMA-DIFFERENTIATED SHCONTROL AND SHTRAF1 THP-1 MACROPHAGES 32
FIGURE 4. ELISA QUANTIFICATION OF IL-1B SECRETION IN PMA-DIFFERENTIATED SHCONTROL AND SHTRAF1 THP-1 MACROPHAGES 34
FIGURE 5. FOLD CHANGE OF IL-1B SECRETION IN PMA-DIFFERENTIATED MACROPHAGES SHCONTROL AND SHTRAF1 THP-1 MACROPHAGES 35
FIGURE 6. CASPASE-1 PROCESSING IN PMA-DIFFERENTIATED SHCONTROL AND SHTRAF1 THP-1 MACROPHAGES 36
FIGURE 7. BIOLUMINESCENT CASPASE-1 ACTIVITY IN PMA-DIFFERENTIATED SHCONTROL AND SHTRAF1 THP-1 MACROPHAGES 38
FIGURE 8. FOLD CHANGE REPRESENTATION OF CASPASE-1 ACTIVITY IN PMA-DIFFERENTIATED SHCONTROL AND SHTRAF1 THP-1 MACROPHAGES 39
FIGURE 9. NLRP3 INFLAMMASOME-DEPENDENT ASC OLIGOMERIZATION IN PMA-DIFFERENTIATED SHCONTROL AND SHTRAF1 THP-1 MACROPHAGES 40
FIGURE 10. LUBAC-MEDIATED ASC LINEAR UBIQUITINATION IN PMA-DIFFERENTIATED SHCONTROL AND SHTRAF1 THP-1 MACROPHAGES 42
FIGURE 11. OPTIMIZED ASSAY TESTING THE FUNCTIONALITY OF DISPLACEMENT AND FLAP-PROBE OLIGOS DESIGNED TO DETECT WT, HETEROZYGOUS, AND SNP IN CLONES USING DESIGNED CONTROL OLIGOS 44
FIGURE 12. GEL IMAGE OF CRISPR/CAS9-MEDIATED CLEAVAGE IN THP-1 CELLS 46
FIGURE 13. SCREENING THP-1 SINGLE-CELL CLONES FOR DETECTION OF HDR EVENTS 47
FIGURE 14. SEQUENCING CHROMATOGRAPHS FOR TRAF1 MUTANT V203 KI IN THP-1 CELLS 49

List of Tables

TABLE 1. ANTISENSE SEQUENCE USED TO CREATE A TRAF1 KNOCKDOWN 13
TABLE 2. LIST OF PRIMERS USED FOR THE FORMATION OF RNP COMPLEX 17
TABLE 3. LIST OF PRIMERS FOR TRAF1 MUTANTS (V203A& S283) AND AAVS1 AND THE RESPECTIVE ANNEALING TEMPERATURES 19
TABLE 4. LIST OF DESIGNED PRIMERS FOR CRISPR/CAS9 HDR-MEDIATED KNOCK-IN SCREENING 23

List of Abbreviations

AIM2	Absent-in-melanoma 2
ALRs	Absent in melanoma 2 (AIM2)-like receptors
ASC	Apoptosis-associated speck-like protein containing a CARD
ATP	Adenosine triphosphate
CAPS	Cryopyrin-associated periodic syndromes
CARD	Caspase recruitment domain
cIAP	Cellular inhibitor of apoptosis protein
CLRs	C-type lectin receptors
CRISPR/Cas9	Clustered Regularly Interspaced Short Palindromic Repeats
crRNA	CRISPR RNA
DAMP	Damage-associated molecular pattern
DNA	Deoxyribonucleic acid
DSB	Double-Stranded Break
E1	Ubiquitin-activating enzyme
E2	Ubiquitin-conjugating enzyme
E3	Ubiquitin ligating enzyme
GSDMD	Gasdermin D
HDR	Homology-Directed Repair
HOIL1	Heme-oxidized IRP2 ubiquitin ligase 1
HOIP	HOIL1-interacting protein
IkB	Inhibitor of kB
IKK	IκB kinase
IL-1	Interleukin-1
IL-1β	interleukin-1β
IL-6	Interleukin-6
IL-12	Interleukin-12
IRF	Interferon-regulatory factors
K48-Ub	K48-linked polyubiquitination
K63-Ub	K63-linked polyubiquitination
LPS	Lipopolysaccharide
LRRs	Leucine-rich repeats
LUBAC	Linear ubiquitin chain assemble complex
MAPK	Mitogen-activated protein kinase
Met1-Ub	Methionine 1-linked ubiquitin
MSU	Monosodium urate
mtROS	Mitochondrial ROS
NEMO	NF-kB essential modulator
NF-κB	Nuclear factor-κB
NHEJ	Non-Homologous End Joining
NLR	Nucleotide-binding oligomerization domain-like receptors
NLRC4	NLR-family CARD domain-containing protein 4
NLRP	Nod-like receptor protein
NLRP1	NLR Family Pyrin Domain Containing 1

NLRP3	NLR family pyrin domain containing 3
NOD	Nucleotide-binding oligomerization domain
NOD2	Nucleotide-binding and oligomerization domain-containing protein 2
P2X7R	P2X purinoceptor 7 receptor
PAMP	Pathogen-associated molecular pattern
PI3K/Akt	Phosphoinositide 3-kinase/Akt
PRR	Pattern-recognition receptor
PYD	Pyrin domain
RIG-I	Retinoic acid-inducible gene I
RLRs	Retinoic acid-inducible gene (RIG)-I-like receptors
RNP	Ribonucleoprotein
ROS	Reactive oxygen species
SgRNA	Synthetic guide RNA
SHARPIN	SHANK-associated RH domain-interacting protein
ShRNA	Short hairpin RNA
SNP	Single nucleotide polymorphism
TIR	Toll/interleukin-1 receptor domain
TLR	Toll-like receptor
TNF	Tumor necrosis factor
TNFR	Tumor necrosis factor receptor
TRAF1	Tumor necrosis factor receptor -associated factor 1
Ub	Ubiquitination
WT	Wild type

Chapter 1: Literature Overview

1.1 Pattern Recognition Receptors

The innate immune system is the first line of host defense activated by the engagement of pattern-recognition receptors (PRRs) that recognize harmful stimuli such as microbial infections, cellular damage, and environmental irritants (1). PRRs are germline-encoded evolutionary conserved sensors expressed on the surface of immune cells that sense molecular structures present in pathogens (pathogen-associated molecular patterns, so-called PAMPs) or endogenous molecules released from damaged cells (damage-associated molecular patterns, so-called DAMPs), leading to an array of immune responses (1–3). To date, five different classes of PRR families have been identified, including transmembrane proteins such as Toll-like receptors (TLRs), C-type lectin receptors (CLRs), in addition to cytoplasmic proteins such as Retinoic acid-inducible gene (RIG)-I-like receptors (RLRs), Absent in melanoma 2 (AIM2)-like receptors (ALRs), and Nucleotide-binding oligomerization domain (NOD)-like receptors (NLRs) (2, 4, 5).

The TLR family is one of the best-characterized forms of PRR families, consisting of N-terminal leucine-rich repeats (LRRs) that mediate recognition of PAMPs, transmembrane domains, and cytoplasmic Toll/interleukin-1 receptor domain (TIR) necessary for downstream signal transduction (6–8). TLRs are responsible for the recognition of different molecular patterns of microbial agents in various cellular compartments, including the plasma membrane, endosome, and lysosomes (4, 9). Moreover, TLRs can lead to activation of a distinct transcription factor referred to as nuclear factor-κB (NF-κB). Upon activation with microbial patterns, multiple signaling cascades are activated that lead to activation of IκB kinase (IKK) comprising two catalytic subunits (IKKα, IKKβ) and a regulatory subunit IKKγ (NEMO) (9, 10). Activation of IKK results in phosphorylation of IκBα and its K48-linked poly-ubiquitination

followed by degradation in the 26S proteasome. This results in translocation of NF-κB from the cytoplasm to the nucleus and binding to promoter elements followed by induction of gene expression of pro-inflammatory mediators and cytokines, such as IL-1, IL-6, IL-12, and TNF-α (11). These cytokines, and chemokines are required to mediate the innate immune response and clearance of the pathogen (12, 13). Additionally, sensing of microbial products and metabolic stressors results in activation of other intracellular signalling pathways including, the PI3K/Akt and RAS/MAPK that are involved in cell survival signalling (14).

Furthermore, NLR, another class of PRRs, plays a crucial role in recognition and defense against microbial agents or extracellular danger signals. NLRs are characterized by the presence of an amino- terminal effector binding domain, a central NACHT domain, and a stretch of carboxy-terminal leucine-rich repeats (LRRs) motifs (15). The amino-terminal protein-interaction domain can be sub-classified into caspase-recruitment domains (CARDs) and pyrin domain (PYD) that are mainly linked to NLR receptor molecules and downstream adaptors and effector proteins. The LRR plays a role in protein-protein interaction and senses the activation signals (PAMP/DAMP) (4, 5, 9). The NATCH domain binds nucleotide and regulates oligomerization and activation of NLR. Activation of NLR by recognition of PAMPs and DAMPs induces inflammatory responses that regulate array of immune processes such as mediating NF-κB, MAPK pathways, and most importantly assembly of the inflammasomes (3, 15).

1.2 Inflammasomes

Inflammasomes are intracellular multi-protein complexes that are a central component of the innate immune system to fight infection (3, 16, 17). These multimeric-protein complexes are mainly expressed in immune cells of myeloid lineage and epithelial cells with mucosal surfaces

(18, 19). Inflammasomes are typically formed of a cytosolic pattern recognition receptor such as NLR or AIM2, the adapter protein ASC, and the effector protein caspase-1 (20). The first family of sensor proteins discovered to form inflammasomes were NLRs, comprised of 22 genes in humans (21). In addition to NLR members (NLRP3, NLRP1, and NLRC4), the ALR and RLR families have been shown to play a role in the formation of inflammasomes (22). Among NLR inflammasome members, NLRP3 is activated in response to a wide array of physically and chemically diverse stimuli unlike other members that require a specific signal. The stimuli include endogenous stress signals such as extracellular adenosine triphosphate (ATP), monosodium urate crystals (MSU), reactive oxygen species (ROS), and exogenous particles like pathogens, pore-forming toxins, and aluminum salts (16, 17, 22, 23).

The assembly of inflammasome complex is dependent on cytosolic sensing of diverse stimuli that are associated with infection (PAMPs) or cellular stress (DAMPs), allowing the formation of the platform for activation of the proteolytic enzyme caspase-1, which in turn regulates the processing of pro-interleukin (pro-IL)-1β to its biologically active form IL- 1β (22, 23).

Since IL- 1β is a very potent cytokine, its secretion is tightly regulated by the assembly of the inflammasome complex before it can be released. This is in contrast to other cytokines such as tumor necrosis factor (TNF), IL-1, IL-6, and many others (24). In fact, studies have shown that dysregulation and excessive production of IL-1β can lead to a number of inflammatory diseases (25–27) .

In addition to cytokine secretion, inflammasome activation results in programmed cell death, referred to as pyroptosis to prevent intracellular replication of the pathogen (28, 29). In addition to their role in host defense against pathogens, inflammasomes have been widely

implicated in the pathogenesis of many autoinflammatory and autoimmune diseases such as gout, rheumatoid arthritis (RA), and lupus (30–34).

1.3 The NLRP3 Inflammasome

To date, the best-characterized and widely studied inflammasome complex is NLPR3. The NLRP3 inflammasome complex consists of NLR cytosolic sensor, ASC containing a caspase-activation and recruitment domain (CARD) adaptor protein, and pro-caspase-1 (35). Upon stimuli recognition, the NLRP3 binds the adaptor protein ASC through pyrin-pyrin domain interaction, promoting ASC oligomerization in filaments that form a large multimeric complex referred to as ASC 'specks'. The oligomerized ASC further recruit pro-caspase-1 through CARD-CARD domain interaction and leads to maturation of pro-caspase-1 via proteolytic cleavage (36). Activate caspase-1 can then proteolytically process pro- IL-1β and pro-IL-18 cytokines to their mature form, which results in the secretion of bioactive cytokines. Moreover, active caspase-1 cleaves a pore-forming molecule called Gasdermin D to induce programmed cell death termed pyroptosis (29, 37).

The activation of NLRP3 involves the integration of two signals that indicate cellular damage or stress. The first signal, referred to as priming is induced by bacterial toxins or PAMPs such as lipopolysaccharide (LPS) that acts on TLR and promotes the NF-κB dependent transcription of NLRP3 and pro-IL-1β prior to inflammasome stimulation (priming step, Signal 1) (17, 28, 38) Nonetheless, other NF-κB activating stimuli such as TNF, Pam3CSK, and IL-1 can be used instead of LPS to prime the cells before stimulation with inflammasome activators (23). However, the NLRP3 inflammasome requires a second signal for assembly and activation. This is achieved by a multitude of pathogens and pathogen-derived molecules that signify stress-associated danger signals (Signal 2) (3, 16, 38). Indeed, a number of mechanisms have been

shown to activate the NLRP3 inflammasome. For example, pore formation is a common process induced by bacterial pore-forming toxins like nigericin that act as a potassium ionophore that disrupt the membrane potential causing potassium efflux leading to NLRP3 activation (39). Similarly, binding of extracellular ATP to P2X7R ATP-gated ion channel triggers potassium efflux and formation of pores in the membrane, mediated by pannexin-1 channel, and thereby activation of NLRP3 (38, 39). Additional activator of NLRP3 includes MSU crystals that are crystallized form of uric acid, which are formed by the precipitation of MSU in the articular joints and tissues leading to gouty arthritis (32). Moreover, mitochondrial reactive oxygen species (ROS) generated in spatial and temporal proximity have been shown to contribute to the activation of the NLRP3 inflammasome (40, 41). For instance, NLRP3 inflammasome inducers such as nigericin, ATP, and MSU can trigger production of ROS, which further activates NLRP3, leading to caspase-1 activation and IL-1β secretion (3, 23, 32, 39).

Many studies have revealed a link between mutations in human NLR genes and various autoimmune and autoinflammatory diseases, signifying the essential role of NLR in the immune system. For instance, cryopyrin-associated periodic syndrome (CAPS) is an autoinflammatory syndrome characterized by self-activation of the NLRP3 inflammasome due to genetic mutation in NLRP3 (42). Such mutation is found within the coding region of the NLRP3 gene and gives rise to continuously active NLRP3 proteins. The severity of the disease depends on the mutation and can vary from mild form characterized by periodic fever flares and skin rash to severe forms, which can be continuous fever flares, hearing loss, and meningitis (23, 43). This shows that increased NLRP3 results in heightened inflammasome activation and thereby leading to an autoinflammatory disorder (44). Furthermore, dysregulation of the NLRP3 inflammasome activation and aberrant IL-1β processing is the driver of other autoinflammatory diseases

including gout, RA, and lupus (24, 25, 31). Previous literature has shown that chronic and excessive activation of NLRP3 inflammasome contributes to the pathogenesis of metabolic disorders such as obesity, type II diabetes, and atherosclerosis (27, 45, 46). Thus, activation of the NLRP3 inflammasome requires a regulatory mechanism to tightly control its activity to prevent excessive inflammation and host damage (24).

1.4 Regulation of Inflammasome

The activation of the NLRP3 inflammasome is essential for host defense against microbial products and invading pathogens (13, 23, 47). However, as discussed, dysregulated inflammasome activation has been implicated in the pathogenesis of various inflammatory diseases (32, 33, 48). Hence, regulation of NLRP3 inflammasome activation is crucial to provide an adequate immune defense. This is achieved by various post-translational modifications including ubiquitination (Ub), phosphorylation (P), sumolyation (S), and s-nitrosylation (SN) (47, 49). Interestingly, it is becoming very clear that the ubiquitin system plays a crucial role in regulating inflammasome activation (50).

Ubiquitination is the best-characterized form of post-translational modification that regulates a multitude of cellular processes such as cell signalling, apoptosis, DNA repair, and immune response (51, 52). The modification of proteins by ubiquitin involves the attachment of one or more ubiquitin to a target protein. Ubiquitin is a highly conserved protein consisting of 76 amino acids with a molecular weight of 8.5 KDa. The conjugation of ubiquitin is mediated by three different classes of enzymes, including the ubiquitin-activating enzyme (E1), the ubiquitin-conjugating enzyme (E2), and the ubiquitin ligating enzyme (E3) (52).

The ubiquitin-activating enzyme E1 is an ATP-dependent process that catalyzes the formation of a thioester bond between the C-terminal carboxyl group of ubiquitin and the cysteine group of

the ubiquitin-activating enzyme E2. Next, E2 catalyzes the transfer of the activated ubiquitin from E1 to the cysteine residue in the active site of the E2. Lastly, E3 ligase mediates the attachment of the lysine residue of the target protein and the C-terminus of ubiquitin by creating an isopeptide bond (53) .

Ubiquitin has seven lysine residues (K6, K11, K27, K29, K33, K48, K63) and a N-terminal methionine (M1) residue that are potential sites for the formation of eight different inter-ubiquitin linkages, resulting in polyubiquitination (52, 54). Among them, the most predominant forms of ubiquitin linkages are K48 and K63 linkages, which account for roughly 80% of the total linkages in mammalian cells (54). K48-linked ubiquitin chains are known to targets proteins for proteasomal degradation, whereas K63- linked chains regulate inflammatory signal transduction, endocytosis, DNA repair, and protein localization (55). Moreover, the novel linear or M1-linked polyubiquitins are essential modulators of innate and adaptive responses by regulating inflammatory cell signalling pathways and their formation is catalyzed by the linear ubiquitin chain assembly complex (LUBAC) (52).

LUBAC is a trimeric complex consisting of three subunits: HOIP, HOIL-1, and SHARPIN, which plays a crucial role in an array of antimicrobial and inflammatory pathways, including TLRs, NLRP3, TNF, and NOD2 (56). Met1-linked linear ubiquitin modification has been shown to regulate NF-κB activation by linear ubiquitination of NEMO (57). In addition to NF-κB regulation, the HOIL-1 subunit of LUBAC mediates linear ubiquitination of ASC adaptor protein leading to the assembly of ASC/NLRP3 complex and subsequent NLRP3 inflammasome activation (49, 56). Thus, tight regulation of LUBAC activity is essential to maintain a balanced and healthy immune response. Interestingly, findings from our lab demonstrated that LUBAC is tightly regulated by TRAF1.

1.5 Multifaceted Roles of TRAF1 in Signalling Pathways

The tumor necrosis factor receptor (TNFR)-associated factors (TRAFs) are a group of genetically conserved adaptor proteins consisting of six family member proteins (TRAF 1-6) (58). TRAFs are major signal transducers for the TNFR, TLR, and NLR signalling pathways (59). Moreover, a wide array of cellular functions such as innate and adaptive responses, tissue homeostasis, bone metabolism, and stress responses are mediated by TRAFs through promoting cell survival, proliferation, differentiation, and death. TRAFs recruitment leads to activation of downstream signalling pathways such as NF-κB, mitogen-activated protein kinases (MAPK), and interferon-regulatory factors (IRF) (59).

TRAF1 is a unique member of the TRAF family as it lacks a RING finger domain that is present in TRAF 2-6. Furthermore, TRAF1 has the most restricted expression among TRAFs, which is limited to activated lymphocytes, dendritic, and myeloid cells (58, 59). Previous literature have indicated opposing roles of TRAF1 downstream of TNFR, TLR, and NOD1/2 immune signalling pathways as both positive and negative regulator of NF-κB activation (60–62). Indeed, TRAF1 plays a context-dependent role by either promoting NF-κB downstream of TNFR in lymphocytes or limiting NF-κB through inhibiting linear ubiquitination downstream of TLR in monocytes.

Most studies have demonstrated that TRAF1 promotes NF-κB activation and thereby survival through forming a heterotrimer with TRAF2 and subsequent recruitment of cIAP1/2 to cytoplasmic tails of TNFR in lymphocytes. On the other hand, a recent study by Abdul-Sater et al. showed that TRAF1 negatively regulates NF-κB activation downstream of TLR signalling by directly interacting with all three components of LUBAC and thereby suppressing its activity.

This, in turn, leads to reduction of LUBAC-mediated NEMO linear ubiquitination and ultimately decreased NF-κB activation (60)

As TRAF1 might also be implicated in inflammasome assembly through LUBAC complex via linear ubiquitination of ASC, understanding the underlying mechanism that regulates NLRP3 inflammasome activation is of utmost importance. This is explained by the vital role of inflammasome in the innate response that has been associated with a multitude of chronic autoinflammatory and autoimmune diseases, such as RA, gout, and lupus (30, 34). Indeed, our group has identified the site of interaction between TRAF1/cIAP2 downstream of TNFR, and TRAF1/LUBAC downstream of TLR using site-directed mutagenesis. It has been signified that mutant variant of TRAF1, including V203A fails to interact with cIAP2 while maintains complete interaction with HOIL-1 subunit of LUBAC. Whereas S283A, another mutant version of TRAF1 fails to bind LUBAC without affecting interaction with cIAP2. Therefore, altering the specific amino acid residues essential for TRAF1 interaction with LUBAC and cIAP2 will allow us to examine how TRAF1 might be regulating NLRP3 inflammasome activation mediated by LUBAC independently of its role in regulating NF-κB activation.

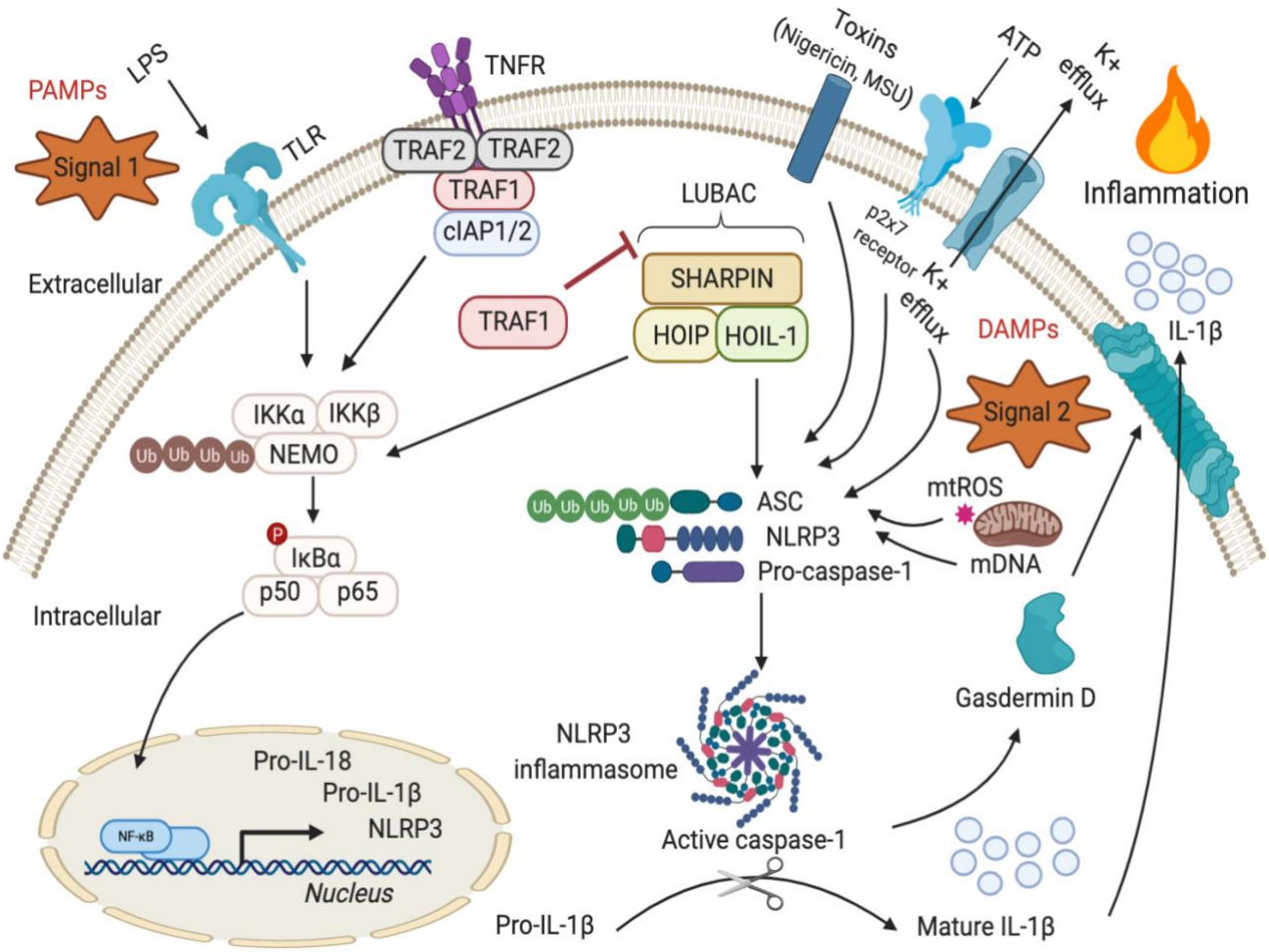

Figure 1. An overview of TRAF1 mediated regulation of NLRP3 inflammasome activation via LUBAC downstream of TNFR.

Chapter 2: Rationale and Objectives

2.1 Rationale

Previous studies have recognized TRAF1 as a negative and positive regulator of several signalling pathways, including TLRs and TNFRs. TRAF1 has been shown to limit linear ubiquitination by directly binding to components of the LUBAC and limiting its activity. Given the importance of linear ubiquitination as a regulatory mechanism in various immune pathways such as ASC linear ubiquitination in the NLRP3 inflammasome and its role in a multitude of autoimmune diseases, it is crucial to examine the role of TRAF1-LUBAC interaction in NLRP3 inflammasome regulation. Moreover, since TRAF1 has been linked with an increased risk of RA, it may also act as a modulator of inflammasome-driven arthritis. Therefore, understanding the underlying mechanism of TRAF1-mediated NLRP3 inflammasome regulation helps ensure a balanced immune response that would prevent autoimmune and autoinflammatory pathologies such as arthritis.

2.2 Objectives

The main objectives of the study are:

1) Assess the role of TRAF1 as a negative regulator of NLRP3 inflammasome via LUBAC
2) Determine the mechanism through which TRAF1 affects NLRP3 inflammasome regulation
3) Create a genetically modified TRAF1 using previously identified amino acid residues that are essential for TRAF1 interaction with LUBAC (S283) and cIAP2 (V203) via CRISPR/Cas9-mediated Homology directed repair (HDR)

2.3 Hypothesis

We hypothesize that TRAF1 limits NLRP3 inflammasome activation by interfering with the linear ubiquitination of ASC. We expect that TRAF1 knockdown cells would exhibit increased NLRP3 inflammasome activation.

Chapter 3: Experimental procedures

3.1 Cell Culture

THP-1 human monocytic leukemia cells were obtained from Sigma-Aldrich. THP-1 cells were cultured in a humidified incubator at 37°C with 5% CO_2 in RPMI 1640 (Sigma-Aldrich) supplemented with 10% heat-inactivated fetal bovine serum (Multicell), 2-Mercapthoethanol (Gibco), 1% L-Glutamine-Pyruvate-Penicillin-Streptomycin (GPPS), and non-essential amino acids (Sigma).

3.2 Lentiviral Transduction for Generation of TRAF1 Knockdown Cells

3.2.1 HEK 293T/17 Transfection

HEK 293T/17 cells (Sigma) were seeded at $2x10^6$ cells per plate in a 6-cm tissue culture treated plates in Dulbecco's modified Eagle's medium (DMEM) (Sigma-Aldrich). Cells were then incubated at 37°C in 5% CO_2 overnight to reach 80-95% confluency. Next day, transfection plasmid mixtures of shControl (3 ug) and shTRAF1 (3 ug) were prepared separately by mixing with 18 ul of TransIT®-Lenti Transfection Reagent (Mirus Bio), psPAX2 (2.4 ug) (Addgene), and VSVG (0.6 ug) (Addgene) in 600 ul of Opti-MEM (Gibco). The mixture was incubated for 10 min at room temperature. Then the transfection mix was carefully added on the cells in a dropwise manner to prevent dislodge of the cells. Next, cells were incubated at 37°C and 5% CO_2 for 48 hrs. The virus was harvested 48 hrs post-transfection by centrifuging cell supernatant at 300 g for 5 min at 4°C. The viral supernatant was collected and filtered through a low-protein-binding 0.22 um filter and added to THP-1 cells for 24 h before selection with 2.5 ug/ml puromycin (Biobasic).

Table 1. Antisense sequence used to create a TRAF1 knockdown

Gene	**Antisense sequence**
TRAF1	AACAATGTTCTCAAACACACG

3.2.2 THP-1 Transduction

THP-1 cells were seeded at 500,000 cells in 500 ul of RPMI 1640 medium in a 12-well tissue culture plate. Then 500 ul of the viral supernatant was added on the cells followed by a 24 hrs incubation in the incubator. Next, the supernatant was removed by centrifugation at 300 g for 5 min. Fresh media with 2.5 ug/ml of puromycin was added to the cells and allowed to grow for the elimination of non-transduced cells.

3.3 Assessing TRAF1 Expression in shControl and shTRAF1 THP-1 Cells

3.3.1 Cellular Treatments

The THP-1 shControl and shTRAF1 cells were seeded at $1.5x10^6$ cells in 1 ml of RPMI in a 12-well plate. Cells were treated with LPS 100 ng/ml for 1, 3, 6, and 24 hrs. At the end of the experiment, cells were collected and transferred into microcentrifuge tubes followed by centrifugation at 300 g for 5 min. The supernatant was removed the cell pellet was washed with ice-cold 1X PBS (Sigma) followed by centrifugation at 300 g for 5 min. The supernatant was removed, and the pellet was resuspended in 100 ul of freshly prepared 1X lysis buffer containing 1% NP- 40 (Igepal CA-630), 100mM Tris pH 8.0, 20% glycerol, 0.2mM EDTA, 150mM NaCl, cOmplete™, Mini, EDTA-free Protease Inhibitor Cocktail (Sigma-Aldrich), 1X Phosphatase Inhibitor Cocktail 3 (Sigma-Aldrich), 1 mM DTT (Sigma-Aldrich), and ddH_2O. The lysates were kept on ice and vortexed every 5 min for total 30 min to ensure cell lysis. The lysates were centrifuged at 14.8 RPM at 4°C and the supernatant was collected in pre-chilled new microcentrifuge tubes. The amount of protein concentration was measured in the lysate using the Bradford Reagent (BioRad).

3.3.2 Bradford Protein Assay

The Bradford protein assay was used to determine the protein concentration of the samples. The Bradford assay was performed in a 96-well flat bottom plate. The Bradford Reagent (1X) was removed from the 4°C storage and let reach room temperature. The bovine serum albumin (BSA) was also removed from -20°C and let thaw on ice. BSA (1 mg/ml) was used as a standard protein to perform a two-fold serial dilution. This was performed by preparing 6 protein standards including 128 ug/ml, 64 ug/ml, 32 ug/ml, 16 ug/ml, 8 ug/ml, and 4 ug/ml. The 128 ug/ml of the standard was prepared in a microcentrifuge tube by adding 872 ul of the 1X Bradford reagent and 128 ul of the BSA (1mg/ml). The mixture was vortexed and 500 ul was transferred into the next microcentrifuge containing 500 ul of the reagent to make a final concentration of 64 ug/ml. The serial dilution continued until the lowest concentration of 4 ug/ml was achieved. The reagent alone was used as a blank for background subtraction. The samples were prepared by adding 5 ul of each sample in a 96-well flat bottom plate followed by addition of 195 ul of the 1X Bradford reagent to achieve a 1:40 dilution of the protein samples. The samples and the reagent were mixed in wells of a flat-bottom 96 well plate by pipetting and the absorbance was measured after 5 min at 595 nm using a plate reader (Verioskan). The concentrations of the unknown protein samples were calculated by plotting a BSA standard curve. The line of best fit and the equation for the standard curve was used to calculate the samples protein concentrations.

3.3.3 Immunoblotting

The protein samples were eluted with 5X Laemmeli Sample Buffer (BioRad) with 2-ME and water to achieve a 1X final protein concentration. The protein samples were heated at 100°C for 5 min and loaded onto a 10% SDS-polyacrylamide to run for 60 V for 30 min followed by

120 V for 90 min. Then the protein samples were transferred to a polyvinyldene difluoride membrane (Bio-Rad). The blot was blocked with 5% skim milk in TBST for 1 h at room temperature. The membrane was incubated with the TRAF1 primary antibody (1:1000) (Cell Signalling 4715) overnight at 4 °C and β-actin primary antibody (1:1000) (R&D Systems Inc. MAB8929) for 1 h at room temperature. Subsequently, the membrane was incubated with peroxidase-conjugated secondary anti-rabbit (1:10,000) and anti-mouse (1:10,000) for 1 h at room temperature for detection of TRAF1 and actin respectively. Immunoreactive proteins were detected with Clarity Max ™ ECL Western blotting detection reagent (Bio-Rad) using ChemiDoc MP imaging system (Bio-Rad).

3.4 CRISPR/Cas9-Mediated Gene Knock-in

3.4.1 Pre-electroporation

THP-1 cells were seeded at 200,000 cells/ml and were incubated in culture for 2-3 days to reach a density of 400,000 cells/ml before nucleofection (Lonza). Cells with high viability (>90%) and in the logarithmic growth phase were used for nucleofection.

3.4.2 RNP Complexing

The crRNA: tracer RNA duplex (sgRNA) for TRAF1-V203A and TRAF1-S283A were prepared by annealing TRAF1-V203 and TRAF1-S283 TrueGuide™ crRNA (100 uM), TrueGuide™ tracrRNA (100 uM) (Dharmacon), and 5X Annealing buffer (Invitrogen) using PCR (BioRad). PCR included an initial denaturation at 95°C for 5 min followed by a step down from 95°C to 78 °C with -2°C increments per second, 78°C for 10 min, 78°C to 25°C with -0.1°C increment per second ramp rate, and lastly 25°C for 5 min.

Next, the RNP complex was formed by combining the TRAF1 sgRNA (V203A & S283A) (120pmol), Altr-Cas9 (104 pmol) (Integrated DNA Technologies) and PBS. The

mixtures were prepared in separate microcentrifuge tubes and were incubated at room temperature for 10-20 min to allow for the formation of the RNP complex.

Table 2. List of primers used for the formation of RNP complex

Primer Name	**Primer Sequence 5'-3'**	**Annealing Temperature (Ta)**
V203A crRNA	AAGCTGCGTGTGTTTGAGAACATTGTTGCTGCCCTCAACAAGGAGGTG GAGGCCTCCCACCTG	78°C
S283 crRNA	CTTCGATGGACTTTCCTGTGGAAGATCACAAATGTCACCAGGCGGTGC CATGAGGCGGCCTGTGGCAGGACCGTCAGCCTCTTCTCC	78°C

3.4.3 Electroporation

THP-1 cells were counted using a hemocytometer to obtain a density of 200,000 cells per condition and transferred to conical tubes followed by centrifugation at 90 g for 10 min at room temperature. The supernatant was removed, and the cells were washed twice with 1X PBS. The pelleted THP-1 cells were resuspended in 20 ul of SG Nucleofector electroporation buffer (Lonza). Next, the prepared V203A & S283 RNP complexes were mixed with their respective single stranded donor DNA templates of V203A (100uM) and S283A (100uM) (Dharmacon), along with Alt-R-Cas9 electroporation enhancer (100 uM) (Integrated DNA Technologies). The prepared mixture was added to the cells resuspended in SG Nucleofector solution. The nucleofection mix was gently mixed and transferred into the Nucleocuvette Vessels and zapped using 4D-Nucleofector™ System (Lonza). Immediately after electroporation, cells were incubated for 10 min at room temperature and added to the pre-warmed RPMI 1640 media. The electroporated cells were transferred into a prepared 96-well plate with pre-warmed media containing Alt-R HDR enhancer (Integrated DNA Technologies). Cells were then cultured in a humidified incubator for 48 hrs before proceeding to genomic cleavage assay and single cell cloning.

3.4.4 Limiting Dilution and Clonal Expansion

The bulk-edited population of THP-1 V203A cells were counted using a hemocytometer and the cell concentration (cells/ml) was calculated. The cells were diluted to a concentration of 0.5-1 cells/100 ul of media, which yielded 1 cell per well in most wells of a 96-well flat bottom plate. Seven full 96-well plates were used that contained single cell per well. The single cells were kept in an incubator at 37°C for clonal expansion for 2-8 weeks. The plates were screened regularly to monitor the growth of the cell colonies using a microscope. When colonies reached 70% confluency, they were transferred into a 24-well plate and topped up with fresh media. Then successful individual clones that had expanded were isolated and analyzed for successful insertion of mutants using the Guide-it Knock-in Screening Kit (Takara Bio).

3.5 CRISPR/Cas9 Genomic Cleavage Detection in the Bulk-edited Population of THP-1 cells

The genomic DNA cleavage of target locus (S283 and V203A) was assessed in the bulk-edited population of THP-1 using GeneArt® Genomic Cleavage Detection Kit (Thermo Fisher). Cells were counted using a hematocytometer to obtain a density of $1.5x10^6$ cells/ml. Next, cells were spun down at 200 g for 5 min at 4°C and the supernatant was carefully removed. The cell pellet was resuspended in 50 ul of Cell Lysis Buffer/Protein Degrader (Thermo Fisher) and transferred to a PCR tube for lysis in a thermal cycler. The program for cell lysis included 68°C for 15 min followed by a 95°C for 10 min. The target site was amplified by preparing a PCR reaction mix, including 2 ul of cell lysate, 1 ul of our designed forward and reverse primer mix (10uM), 25 ul AmpliTaq Gold® 360 Master Mix, and 22 ul water. The PCR reaction program consisted of the following steps: enzyme activation (95°C), denaturation (95°C), annealing (55°C), elongation (72°C) and final extension (72°C) for 10 min, 30 sec, 30 sec, 30 sec, and 7 min respectively. Next, 3 ul of the DNA products from the PCR reaction was mixed with 10 ul of

water and fractioned on a 2% agarose gel for one and a half hour at 70 V. The PCR product was verified using a gel imager to detect a single band of correct size. This was followed by the cleavage assay that served to denature and anneal the PCR reaction products to allow for the formation of heteroduplex between the PCR products with and without the indels. Thus, 2 ul of PCR product was mixed with 1 ul 10X Detection Reaction Buffer in a PCR tube and was placed in a thermal cycler. The program included 95°C for 5 min followed by a step down from 95°C to 85°C at -2°C/sec rate, and 85°C to 25°C at -0.1°C/sec rate. Next step included cleavage of the heteroduplex DNA containing the mismatches by addition of 1ul of Detection Enzyme to each sample followed by incubation at 95°C for 1 h. Lastly, the entire 10 ul of PCR reaction mixtures were fractioned on a 2% agarose gel. The bands were analyzed by gel imager for presence of cleaved parental bands.

Table 3. List of primers for TRAF1 mutants (V203A& S283) and AAVS1 and the respective annealing temperatures

Primer Name	Forward Primer Sequence 5'-3'	Forward Primers Sequence 5'-3'	Annealing Temperature (Ta)
TRAF1V203A	CAGAACCTGTCAGACCTGCA	TCAAGCAAAGGAACCGAAGC	55°C
TRAF1S283A	TACAGGTGGTGGAGCTTCAG	ATTCAGGGAGGAGAAAGGGC	55°C
AAVS1	GAATATGTCCCAGATAGCAC	GTTCTCAGTGGCCACCCTGC	55°C

3.6 CRISPR/Cas9 HDR-mediated Knock-in Detection in Positive Control Oligos

The Guide-it Knock-in Screening Kit was used to screen for a successful homology-directed repair and a detection of our desired single-nucleotide substitutions in the bulk edited population and single-clones of THP-1 cells. The protocol overview constituted of designing the displacement, flap-probe, and control oligos (60-90 bp in length) based on the target sequence encoding the wild-type and mutated sequence referring to manufacturer's primer design tool.

3.6.1 Annealing Designed Control Oligos with Displacement and Flap-probe Oligos

First, reactions were performed to test the design of displacement oligos and flap-probe oligos. Moreover, the Guide-it Knock-in Control set provided in the kit was used to ensure the functionality of qPCR machine for detecting the signals generated by Guide-it green and red flap detectors. First, designed wild-type and SNP control oligos, displacement oligos, and flap-probe oligos were resuspended in RNAase-free water to achieve a final concentration of 1 nM, 1 uM, and 20 uM respectively. Next, a heterozygous positive control was prepared by mixing wild-type and SNP control in equal volume for a final concentration of 0.5 nM. In a 384-well plate, 10 ul of wild-type, SNP control oligo, heterozygous positive control, and water (non-template control) were pipetted per well. Subsequently, an annealing master mix consisting of Flap-probe oligos, displacement oligo, annealing buffer, and RNAase-free water were prepared in a 200 ul PCR tube. Then, 5 ul of the prepared annealing master mix was added to each well containing wild-type control oligo, SNP control oligo, heterozygous positive control, and water. Also, 15 ul of Guide-it Knock-in positive control mix and Guide-it Knock-in negative control mix that were provided in the kit were added to separate wells to serve as additional controls. Next, the plate was tightly sealed with an optical film and centrifuged at 700 g for 1 min. Lastly, using a q-PCR machine (Bio-Rad), the wild-type and SNP control oligos were annealed with displacement and flap-probe oligos. The program included 95°C for 5 min followed by a step down from 95°C to 63°C at 0.1°C/sec rate, and 63°C for 10 min.

3.6.2 Performing Enzymatic Reaction for Testing Positive Control Oligos

First, an enzymatic reaction master mix consisting of Guide-it green flap detector, Guide-it red flap detector, flapase enzyme, and flapase buffer were prepared. In a new 384-well plate, 5

ul of the enzymatic reaction master mix was pipetted into the same wells as the annealing reactions plate from section *3.6.1.* Next, the plate containing the annealing reaction in section *3.6.1* was removed from the q-PCR machine, and its contents were transferred to the plate containing the enzymatic reaction master mix. The plate was tightly sealed with an optical film and centrifuged at 700 g for 1 min. Lastly, the plate was placed in a q-PCR machine to read green and red fluorescence. The program consisted of a 63°C for 75 min followed by green and red fluorescent measurements.

3.6.3 Testing Clonal Cell Lines for CRISPR/Cas9 HDR-mediated Knock-in

The clonal cells were counted using a hemocytometer to obtain a density of $1x10^5$ cells and were transferred into a 96-well rounded bottom plate. Then the plate was centrifuged at 300g for 5 min, and the media was removed. The cells were washed twice with 100 ul of PBS-/- followed by the addition of 50 ul of MightyPrep Reagent lysis buffer to each well. The plate was tightly sealed using an optical film and placed in a PCR machine to lyse for 10 min at 95 °C. Next, the plate was centrifuged at 1200 g for 10 min and the supernatant containing the genomic DNA was carefully removed from each well and transferred into a new 96-well plate.

3.6.4 Amplification of the Target Site

A PCR reaction mixture was prepared to amplify our desired target site. The PCR mixture comprised of forward (10 uM) and reverse primer (10 uM), polymerase, 2X reaction buffer, and RNAase- free water. Next, 23 ul of the prepared PCR mixture was added into a 96-well plate containing 2 ul of genomic DNA extracted in section *3.6.3*. Next, an optical film was used to seal the 96-well PCR plate tightly. Then the plate was centrifuged at 700 g for 1 min. Lastly, using a PCR machine the target site was amplified for 2 min at 98°C followed by 35 cycles of 98°C for 10 sec and 68°C for 1 min, and infinite hold at 4°C.

3.6.5 Annealing of PCR Products with Displacement and Flap-probe Oligos

The PCR products prepared in section *3.6.4* were diluted 1/40 using a dilution buffer. Same procedure explained in section *4.1.a* was implemented to anneal PCR products with displacement and flap-probe oligos designed for S2083A and V203A mutations.

3.6.6 Performing Enzymatic Reaction for Testing the Clonal Cell Lines

The enzymatic reaction mixture was prepared as described in section *3.6.1*. Next, 5 ul of the enzymatic reaction master mix was added into a 96-well plate. Next, 10 ul of the annealing reaction mixture of V203A generated from section *3.6.2* were transferred into the plate containing the enzymatic reaction mixture. The plate was covered with an optical film and centrifuged at 700 g for 1 min. Next, the plate was placed in the PCR machine as described previously for further measurements.

Table 4. List of designed primers for CRISPR/Cas9 HDR-mediated knock-in screening

Primer Name	**Primer Sequence 5'-3'**	**Annealing temperature (Ta)**
V203A SNP Control Oligo	AGGCCTCCACCTCCTTGTTGAGGGCAGCAACA ATGTTCTCAAACACACGCAGCTTCCC	63°C
V203A WT Control Oligo	AGGCCTCCACCTCCTTGTTGAGGACAGCAACA ATGTTCTCAAACACACGCAGCTTCCC	63°C
S283A SNP Control Oligo	GGCTGACGGTCCTGCCACAGGCCGCCTCATGG CACCGCCTGGTGACATTGGTGATCTT	63°C
S283A WT Control Oligo	GGCTGACGGTCCTGCCACAGGCCGACTCATGG CACCGCCTGGTGACATTGGTGATCTT	63°C
V203A Displacement	CTGCGTGTGTTTGAGAACATTGTTGCTGA	63°C
S283A Displacement	GTCACCAGGCGGTGCCATGAGC	63°C
V203A Flap probe SNP	ACGGACGCGGAGCCCTCAACAAGGAGGTG/3C6/	63°C
V203A Flap probe WT	AGGCCACGGACGTCCTCAACAAGGAGGTG/3C6/	63°C
S283A Flap probe SNP	ACGGACGCGGAGGCGGCCTGTGGC/3C6/	63°C
S283A Flap probe WT	AGGCCACGGACGTCGGCCTGTGGCA/3C6/	63°C

3.7 Detection of Inflammasome Activation

3.7.1 Cellular Stimulation

For examining the IL-1β and caspase-1 processing by western blot, cells were primed with 100 ng/ml of LPS for 3 hrs in RPMI media followed by 1 and 3 hrs of stimulation with ATP (5 mM) and Nigericin (10 uM) in Opti-MEM I reduced serum media (Life Technologies). Cells were treated with MSU for 6 hrs (250 ug/ml) in Opti-MEM I reduced serum media. Moreover, the supernatant was collected and kept at -80°C for further analysis of caspase-1 activity and IL-1β secretion using Caspase-Glo® 1 Reagent (Promega) and IL-1β ELISA (Thermo Fisher) kits respectively.

For western blot detection of ASC oligomerization, cells were stimulated with 500 ng/ml LPS in 1 ml of RPMI for 4 hrs followed by treatments of nigericin (10 uM) and ATP (5 mM) for 30 min and 1 h in Opti-MEM I reduced serum media respectively. For detection of ASC linear ubiquitination by western blot, cells were treated with LPS (100ng/ml) for 3 hrs followed by nigericin stimulation of 5, 15, 30 min, and 1 h in RPMI to induce NLRP3- mediated inflammasome activation.

3.7.2 Bioluminescent Caspase-1 Activity

After stimulation, 38 ul of the cell supernatant was transferred into a white flat bottom 96-well plate (Greiner bio-one). Then 38 ul of Caspase-Glo® 1 Reagent was added to each sample. Next, the plate contents were mixed using a plate shaker at 300-500 rmp for 30 sec and incubated for 1 h at room temperature. Luminescence was measured using a plate-reader luminometer (Verioskan).

3.7.3 Enzyme Linked Immunosorbent Assay (ELISA)

The IL-1β human uncoated ELISA kit was used to perform quantitative enzyme linked immunosorbent assays (ELISA) to detect and quantify protein levels of IL-1β in the supernatant of stimulated cells. First, the anti-human IL-1β capture antibody (100 ul/well) was immobilized on high protein-binding ELISA 96-well plates (Greiner bio-one) by overnight incubation at 4°C. Then the wells were aspirated and washed three times with wash buffer consisting of PBS-Tween. The plate was blocked with 200 ul of 1X ELISA/ELISPOT diluent to prevent nonspecific binding and was incubated for 1 h at room temperature. Again, the plate was aspirated and washed three times with the wash buffer. The protein standard provided in the kit was used to make a standard curve of 2-150 pg/mL by performing a 2-fold serial dilution in the 1X ELISA/ELISPOT diluent. Dilutions of the cell supernatants were prepared for different treatments of nigericin (1:500), ATP (1:10), and MSU (1:10) in 1X ELISA/ELISPOT diluent to ensure they fall within the linear range of the standard curve. Then 100 ul of pre-diluted cell supernatant and the prepared standards were added to the plate and incubated overnight at 4°C. Next day, the plate was aspirated and washed three-five times, followed by the addition of 100 ul/well of biotin-conjugated anti-human IL-1β antibody for 1h at room temperature. The plate was aspirated and washed three-five times. The Avidin-horseradish peroxidase (HRP) conjugate (100ul/well) was added to the plate and was incubated for 30 min at room temperature. The plate was aspirated and washed three-five times prior to the addition of 100ul of 1X Tetramethylbenzidine (TMB), the substrate for HRP, followed by a 15 min incubation. Lastly, 100 ul/well of the stop solution was added to each sample and absorbance was measured at 450

nm and 750 nm. The values of 570 nm were subtracted from those of 450 nm and the data was analysed.

3.7.4 Detection of IL-1β and Caspase-1 by Western Blot

In order to concentrate proteins for analysis after cell stimulation, the supernatant was collected in microcentrifuge tubes. Then, 100% Trichloroacetic acid (TCA) was added to each sample to bring the TCA concentration to 10%. Samples were vortexed for three-four seconds, followed by a 10 min incubation on ice. Then samples were centrifuged for 10 min at 14.8 RPM at 4°C, and the supernatant was carefully removed leaving protein pellet intact. Next, 45 ul of 1X Laemmli buffer was added to dissolve the protein pellet as the sample turned yellow in color. Hence, small amounts of 1M NaOH was added until the color turned blue. The protein samples were boiled at 95°C for 5 min. Next, samples were loaded onto a 12% SDS-polyacrylamide gel and transferred to a polyvinyldene difluoride membrane (Bio-Rad). Blots were blocked with 5% skim milk in TBST for 1 h at room temperature. Then the membranes were probed for caspase-1 primary antibody (1:1000) (Millipore 06-503-I) and Human IL-1β primary antibody (1:1000) (R & D systems MAB601-SP) and were incubated overnight at 4 °C. Subsequently, the membranes were incubated with peroxidase-conjugated secondary anti-rabbit (1:10,000) and anti-goat (1:10,000) for 1 h at room temperature. Immunoreactive proteins were detected with Clarity Max ^{TM} ECL Western blotting detection reagent (Bio-Rad) using ChemiDoc MP imaging system (Bio-Rad).

3.8 ASC Oligomerization Assay

3.8.1 Western Blot

Cells were seeded at 1.5×10^6 in 1 ml of RPMI 1640 media in a 12-well plate and differentiated with 100 nM PMA overnight. First, cells were washed twice with ice-cold PBS followed by the addition of 500 ul of 1X ASC polymerization lysis buffer containing 2X ASC lysis buffer,

protease inhibitor, and ddH_2O. The 2X ASC polymerization lysis buffer comprised of 40mM HEPES-KOH pH 7.4, 300mM KCl, 2% IGEPAL (NP40), and ddH_2O. Cells were scraped off in lysis buffer and transferred into 1.5 ml microcentrifuge tubes to further shear the cell lysate using a 21G needle. Then 20 ul of each cell lysate was collected as input control of the ASC isolation. The remainder of the cell lysates was centrifuged at 3400 g for 15 min at 4°C. The supernatant was removed, and the pellet was washed three times with 1 ml of PBS. Then 10 ul of freshly prepared 100 mM cross-linker DDS solution (Sigma) dissolved in DMSO (Sigma) was added to the pellets resuspended in 500 ul of PBS and were incubated for 30 min on a rotating shaker at room temperature. Next, the samples were centrifuged for 10 min at 5000 g at 4°C to separate the unbound DDS from the pellets. To prepare the samples, each pellet was resuspended in 35 ul of 2X Laemmli buffer and boiled for 5 min at 95°C. Also, 10 ul of the 2X Laemmli buffer was added to 10 ul of collected cell lysate to serve as input and boiled for 5 min at 95°C. Samples and input were loaded onto a 10% and 13.5% SDS- polyacrylamide gel and transferred to a polyvinylidene difluoride membrane (Bio-Rad). Blots were blocked with 5% skim milk in TBST for 1 hour at room temperature. Then the membranes were probed for ASC/TMS Rabbit PolyAb (1:1000) (Proteintech 10500-1-AP) and β-actin primary antibody (1:1000) (R&D Systems Inc. MAB8929) and incubated overnight at 4 °C. Subsequently, the membranes were incubated with peroxidase-conjugated secondary anti-rabbit (1:10,000) and anti-mouse (1:10,000) for 1 h at room temperature. Immunoreactive proteins were detected with Clarity Max ^{TM} ECL Western blotting detection reagent (Bio-Rad) using ChemiDoc MP imaging system (Bio-Rad).

3.9 Immunoprecipitation

3.9.1 Linear Ubiquitin Chains and ASC

The shControl and shTRAF1 Cells were seeded at $1.5x10^7$ in a 10-cm tissue culture dishes and differentiated using 100 nM PMA overnight. The PMA-differentiated shControl and shTRAF1 cells were primed with LPS followed by nigericin stimulation as described in section 3.7.1. After the completion of the experiment, cells were washed twice with ice-cold PBS and lysed with 800ul of linear ubiquitination IP buffer (7 M urea, 135 mM NaCl, 1% Triton X-100, 1.5 mM $MgCl_2$, 2 mM *N*-ethylmaleimide) containing cOmplete™, Mini, EDTA-free Protease Inhibitor Cocktail, phosphatase inhibitor cocktail 3, and 1 mM DTT at room temperature. The lysates were transferred into microcentrifuge tubes and vortex every 5min for 30 min on ice. Next, the lysates were centrifuged at 14.8 RPM for 15 min and the supernatant was collected in new microcentrifuge tubes. 20 ul of the WCE was kept at -20°C to serve as input for the IP. The lysates (800ul) were incubated with 25 µl of prewashed Pierce™ Protein A/G Agarose beads (Thermo Fisher, 20421) and 2.5 µg linear ubiquitin antibody (clone 1F11/3F5/Y102L, obtained under MTA from Genentech) at room temperature on a rotator overnight to pull down only linearly ubiquitinated ASC (63, 64). Then, the samples were washed five times with linear ubiquitin lysis buffer followed by two washes with 1X PBS. The beads were eluted in 30 ul of 2X LDS reducing sample buffer (BioRad) containing 5mM DTT. The inputs were eluted in 2X LDS reducing sample buffer for a total of 20ul. The input and samples were heated at 70°C for 10 min. The beads were centrifuged, and the supernatant was transferred into new microcentrifuge tubes. The input and the protein samples were subjected to immunoblotting and separated on SDS-PAGE gradient gel 4-15%. The proteins were transferred to a nitrocellulose membrane by wet transfer for 2 h at 30 V. The membrane was blocked in 5%

milk/TBST 0.05 for 1 h at room temperature to avoid non-specific binding. The membrane was washed three times with 1X TBST for 5'min followed by incubation with the ASC/TMS Rabbit PolyAb (Proteintech) primary antibody (1:1000) for 1 h at room temperature. The membrane was washed three times with 1X TBST for 5'min and probed with the secondary anti-rabbit antibody (1:10,000) for 1h. Lastly, SuperSignal™ West Femto Maximum Sensitivity Substrate was used to detect immunoreactive proteins using ChemiDoc MP imaging system.

3.10 Statistical Analysis

Groups were compared for significance using two-way ANOVA (two-tailed) and Šidák's multiple comparison test by GraphPad Prism 4.0. A $p<0.05$, $p<0.01$, and $p<0.001$ were considered as significant. Data are reported as mean ± SEM.

Chapter 4: Results

4.1 Knocking Down TRAF1 Expression in THP-1 Cells

To examine the role of TRAF1 in the regulation of NLRP3 inflammasome activation, a cell line with low TRAF1 levels was required. Thus, we used human monocytic THP-1 cells to create a bulk knockdown of TRAF1 using short hairpin RNA (shRNA) lentiviral transduction method. This involved overexpression of shRNA to target TRAF1 mRNA to generate TRAF1 knockdown (shTRAF1). As a control, we overexpressed an shRNA that had no targets in the human or mouse genomes (shControl). Next, to ensure that TRAF1 was knocked down and its expression was reduced, we stimulated the cells with LPS. This was crucial as the expression of TRAF1 is not detected at basal levels, and its expression is increased upon activation through the NF-κB pathway. Figure 2 demonstrates a Western Blot analysis of TRAF1 expression in shControl and shTRAF1 in the THP-1 cell line. In shControl cells, which contain the same levels of TRAF1 as the wild type, there was increased expression of TRAF1 with 1, 3, 6, and 24 hrs of LPS treatment. In contrast, in shTRAF1 cells, there was a significant reduction in TRAF1 levels upon stimulation with LPS treatment for 1, 3, 6, and 24 hrs compared to shControl. Next, we used shTRAF1 cells to examine the underlying mechanism by which reduced TRAF1 impacts NLRP3 inflammasome activation.

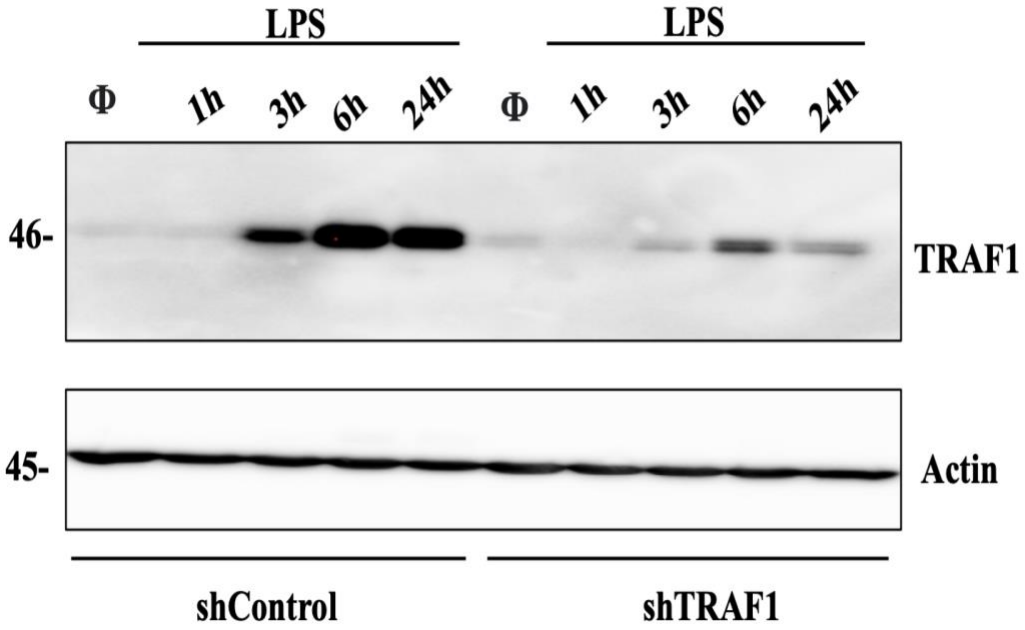

Figure 2. TRAF1 knockdown expression in THP-1 cells
Human monocytic THP-1 shControl and shTRAF1 cells were treated with LPS (100 ng/ml) for the 1, 3, 6, 24 hrs. The whole cell extracts (WCE) from shControl and shTRAF1 were obtained, and protein concentrations were measured using Bradford Assay. The WCE was immunoblotted for TRAF1 and loading control (β-actin). The data shown are representative of three independent experiments.

4.2 Reduced TRAF1 Levels Lead to Increased IL-1β Processing

To test whether TRAF1 regulates the NLRP3 inflammasome, we looked at the expression of IL-1β, a downstream product of NLRP3 inflammasome activation and a critical regulator of inflammation. We used shControl and shTRAF1 THP-1 cells and differentiated them into macrophages using PMA overnight. We used monocyte-derived macrophages as they are considered the first line of defense upon exposure to infection and viral agents and thereby served as a suitable cell line for the purposes of inflammasome activation. Next, we primed the cells with LPS for 3 hrs (Signal 1) followed by stimulations with nigericin and ATP for 1 and 3 hrs that functioned as the second signal required for NLRP3 inflammasome activation. Also, the PMA-differentiated macrophages were stimulated with MSU for 6 hrs. According to Figure 3, the 37 KDa pro-IL-1β was proteolytically cleaved into the bioactive 17 KDa mature IL-1β form.

As shown in the Western Blot analysis, there was increased processing of IL-1β upon stimulation with NLRP3 inducers in TRAF1 knockdown cells compared to control cells as shown by the intensity of the bands (Figure 3). The expression of mature IL-1β was more robust upon stimulation with nigericin and MSU than ATP. Even though ATP stimulation was less potent than nigericin and MSU, it still slightly induced processing of IL-1β in shTRAF1 compared to shControl cells.

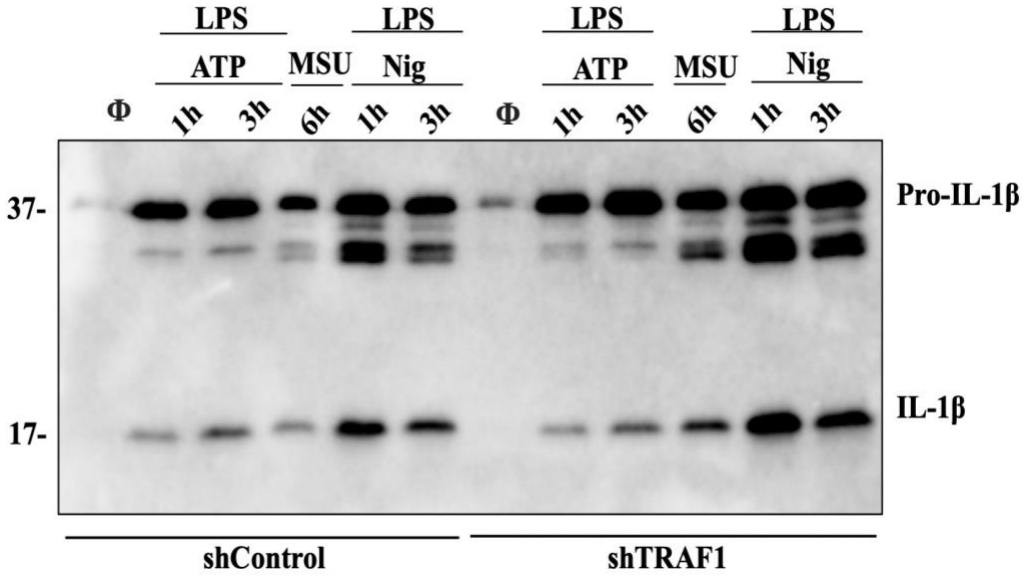

Figure 3. IL-1β processing in PMA-differentiated shControl and shTRAF1 THP-1 macrophages

Human monocytic shControl and shTRAF1 THP-1 cells were differentiated into macrophages using PMA (100 nM) overnight. The PMA induced macrophages were treated with LPS (100 ng/ml) for 3 hrs prior to stimulations with ATP (5 mM) and Nigericin (10 uM) for 1 and 3 hrs. The PMA induced macrophages were treated with MSU (250 ug/ml) for 6 hrs. The culture supernatants were collected, the proteins in the supernatant were precipitated using 100% TCA and immunoblotted for expression of cleaved and uncleaved IL-1β. The data shown are representative of four independent experiment

4.3 Reduced TRAF1 Levels Lead to Increased IL-1β Secretion

In order to quantitively measure IL-1β secretion, the concentration of mature IL-1β was measured as a biomarker of NLRP3 inflammasome activation by ELISA. PMA-differentiated shControl and shTRAF1 cells were treated the same way as described in section 4.2 to induce NLRP3 inflammasome activation. Figure 4 is a representative experiment indicating IL-1β concentration after stimulation with nigericin (1 and 3 hrs), ATP (1 and 3 hrs), and MSU (6 h). Due to variation among independent experiments, we opted to show the fold change increase in the amount of IL-1β with respect to control as shown in Figure 5. Indeed, there was a significant difference in IL-1β levels between shTRAF1 and shControl cells for treatments of nigericin, ATP, and MSU respectively ($p<0.001$, $p<0.01$, $p<0.05$) (Figure 5). The data showed a significant increase in IL-1β secretion for TRAF1 knockdown cells compared to control cells, which is consistent with the Western Blot analysis findings. Therefore, TRAF1 knockdown cells exhibited increased concentration of mature IL-1β compared to controls cells, signifying increased NLRP3 inflammasome activation. Lastly, to further understand the role of TRAF1 on the regulation of NLRP3 inflammasome activation, we looked at caspase-1, the upstream regulator of IL-1β secretion.

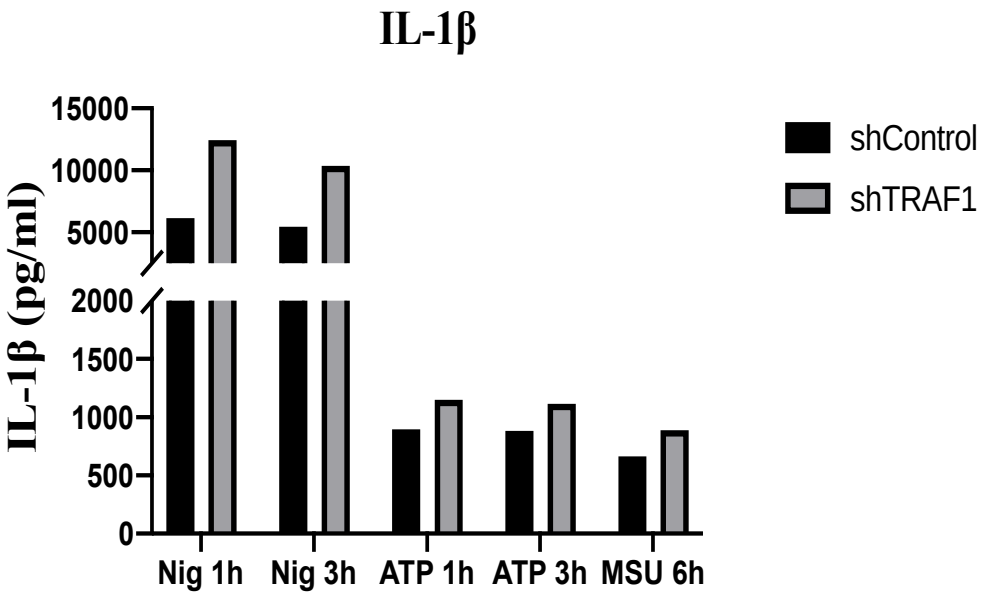

Figure 4. ELISA quantification of IL-1β secretion in PMA-differentiated ShControl and ShTRAF1 THP-1 macrophages

Human monocytic shControl and shTRAF1 THP-1 cells were differentiated into macrophages using PMA (100 nM) overnight. The PMA induced macrophages were treated with LPS (100 ng/ml) for 3 hrs prior to stimulations with ATP (5 mM) and nigericin (10 uM) for 1 and 3 hrs. The PMA induced macrophages were treated with MSU (250 ug/ml) for 6 hrs. Culture supernatant was collected and analyzed for secretion of mature IL-1β by ELISA. The data shown are representative of six independent experiments.

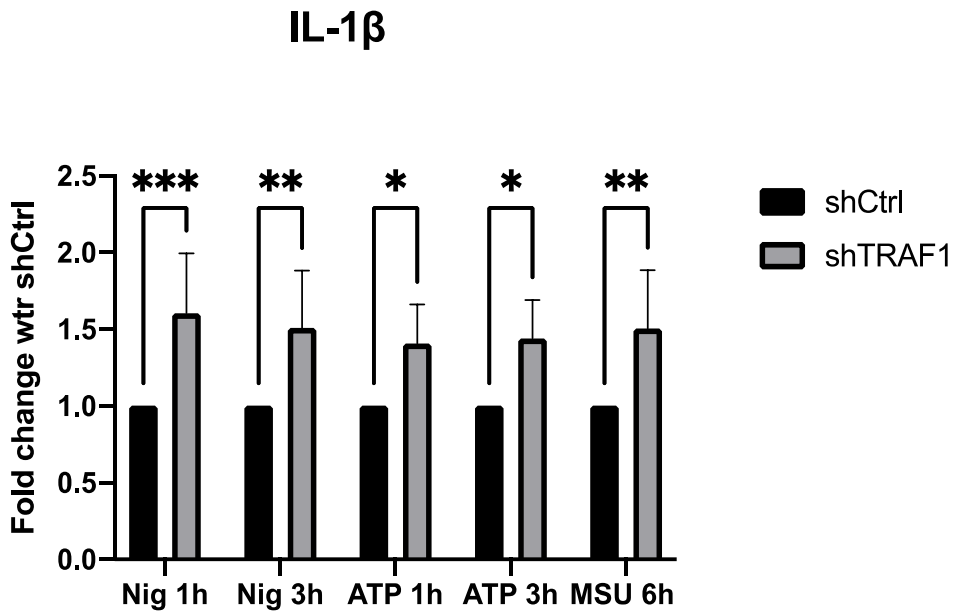

Figure 5. Fold change of IL-1β secretion in PMA-differentiated macrophages shControl and shTRAF1 THP-1 macrophages

Human monocytic shControl and shTRAF1 THP-1 cells were differentiated into macrophages using PMA (100 nM) overnight. The PMA induced macrophages were treated with LPS (100ng/ml) for 3 hrs prior to stimulations with ATP (5 mM) and nigericin (10 uM) for 1 and 3 hrs. The PMA induced macrophages were treated with MSU (250 ug/ml) for 6 hrs. Culture supernatant was collected and analyzed for the secretion of mature IL-1β by ELISA. Values are means and standard deviations. The data shown are representative of six independent experiments. *=p< 0.05, **=p<0.01, ***=p<0.001 by two-way ANOVA.

4.4 Reduced TRAF1 Levels Lead to Increased Caspase-1 Activation

To investigate the role of TRAF1 on the regulation of NLRP3 inflammasome activation, we looked at caspase-1, which is responsible for cleaving pro-caspase-1 to mature caspase-1. To characterize caspase-1 activation, PMA-differentiated shControl and shTRAF1 cells were primed with LPS and stimulated with nigericin and ATP for 1 and 3 hrs. According to Figure 6, the 45-KDa pro-caspase-1 (inactive zymogen) was cleaved into 33 KDa active caspase-1 (37). As demonstrated in the Western Blot analysis, there was increased processing of caspase-1 upon stimulation with NLRP3 inducers in TRAF1 knockdown cells compared to control cells as indicated by the intensity of the bands. Moreover, the expression of caspase-1 was more robust

upon stimulation with nigericin than ATP. Therefore, the results demonstrated that TRAF1 reduces caspase-1 processing compared to the control cells.

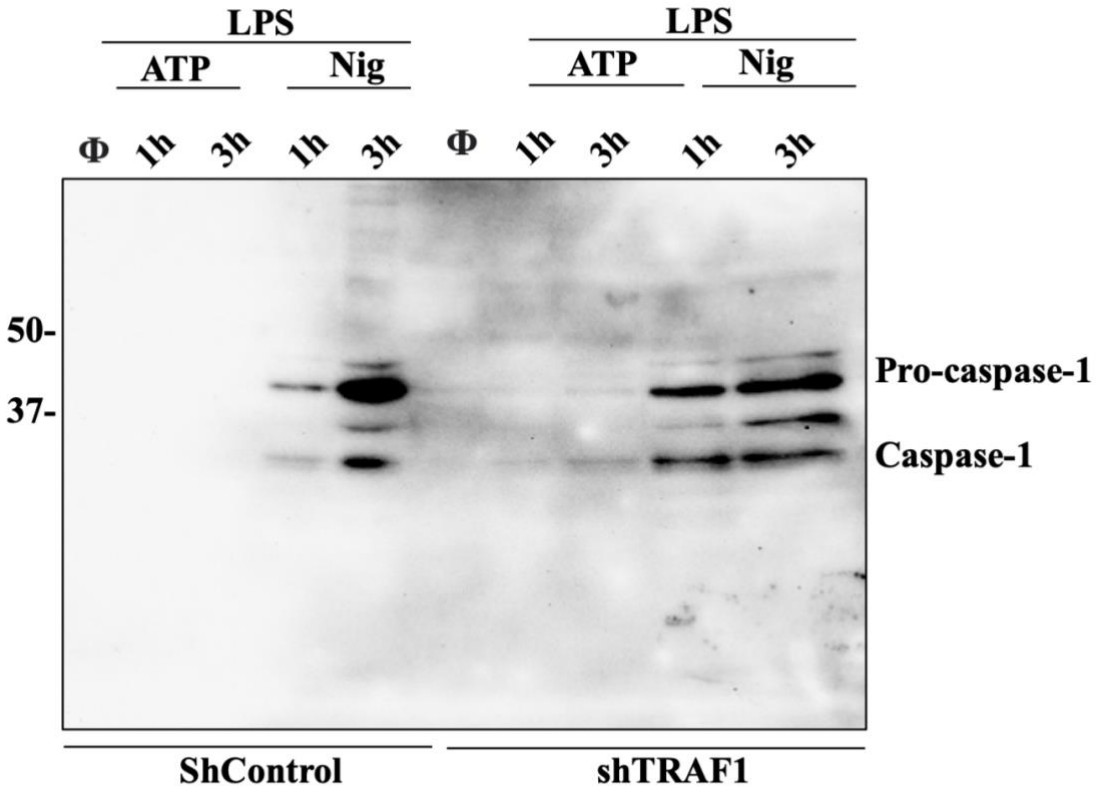

Figure 6. Caspase-1 processing in PMA-differentiated shControl and shTRAF1 THP-1 macrophages

Human monocytic shControl and shTRAF1 THP-1 cells were differentiated into macrophages using PMA (100 nM) overnight. The PMA induced macrophages were treated with LPS (100 ng/ml) for 3 hrs prior to stimulations with ATP (5 mM) and nigericin (10 uM) for 1 and 3 hrs. The culture supernatants were collected, the proteins in the supernatant were precipitated using 100% TCA and immunoblotted for expression of cleaved and uncleaved caspase-1. The data shown are representative of four independent experiments.

4.5 Reduced TRAF1 Levels Lead to Increased Caspase-1 Enzymatic Activity

In order to quantitively measure caspase-1 levels, caspase-1 activity was measured as an indicator of NLRP3 inflammasome activation using a bioluminescence assay. The assay provided a luminogenic caspase-1 substrate (Z-WEHD-aminoluciferin) that was cleaved by the active caspase-1 and yielded a luminescent signal, which corresponded to caspase-1 activity. The PMA-differentiated shControl and shTRAF1 cells were primed with LPS followed by stimulations with nigericin, ATP, and MSU to induce NLRP3 inflammasome activation. Figure 7 is a representative experiment indicating caspase-1 levels after stimulation with nigericin (1 and 3 hrs), ATP (1 and 3 hrs), and MSU (6 hrs). Due to variation among independent experiments, we opted to show the fold change increase in the amount of caspase-1 with respect to control as shown in Figure 8. We found a significant increase in caspase-1 levels in TRAF1 knockdown cells compared to control cells upon stimulations with nigericin (1 and 3 hrs) ($p<0.001$, $p<0.01$) ATP 1 h ($p< 0.05$), and MSU 6 hrs ($p<0.01$). Also, there was increased caspase-1 levels with ATP stimulation of 3 hrs in TRAF1 knockdown cells compared to control cells, but it was not significant. Next, we investigated the mechanism through which TRAF1 is controlling inflammasome activation.

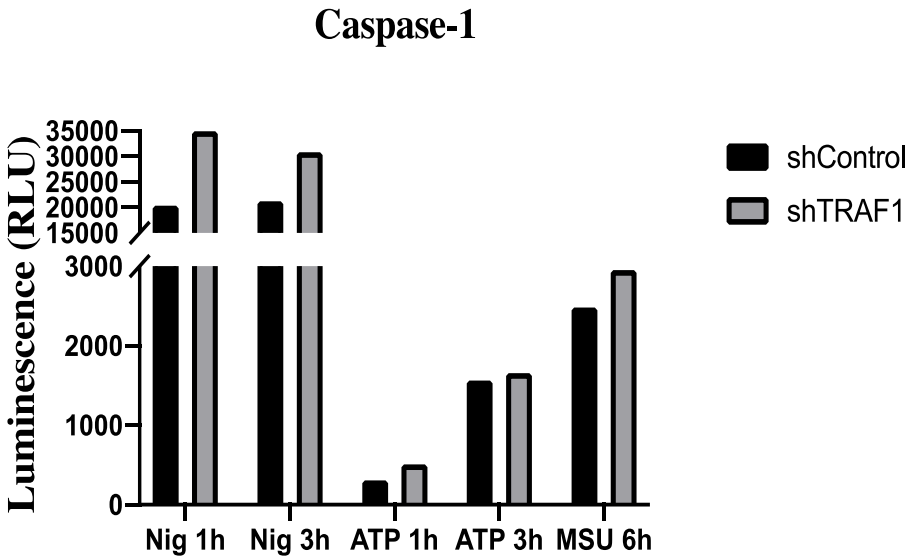

Figure 7. Bioluminescent caspase-1 activity in PMA-differentiated shControl and shTRAF1 THP-1 macrophages

Human monocytic shControl and shTRAF1 THP-1 cells were differentiated into macrophages using PMA (100 nM) overnight. The PMA induced macrophages were treated with LPS (100 ng/ml) for 3h prior to stimulations with ATP (5 mM) and nigericin (10 uM) for 1 and 3hrs. The PMA induced macrophages were treated with MSU (250 ug/ml) for 6hrs. Culture supernatant was collected and analyzed for caspase-1 activity by Caspase-Glo® 1 Inflammasome Assay. The data shown are representative of four independent experiments.

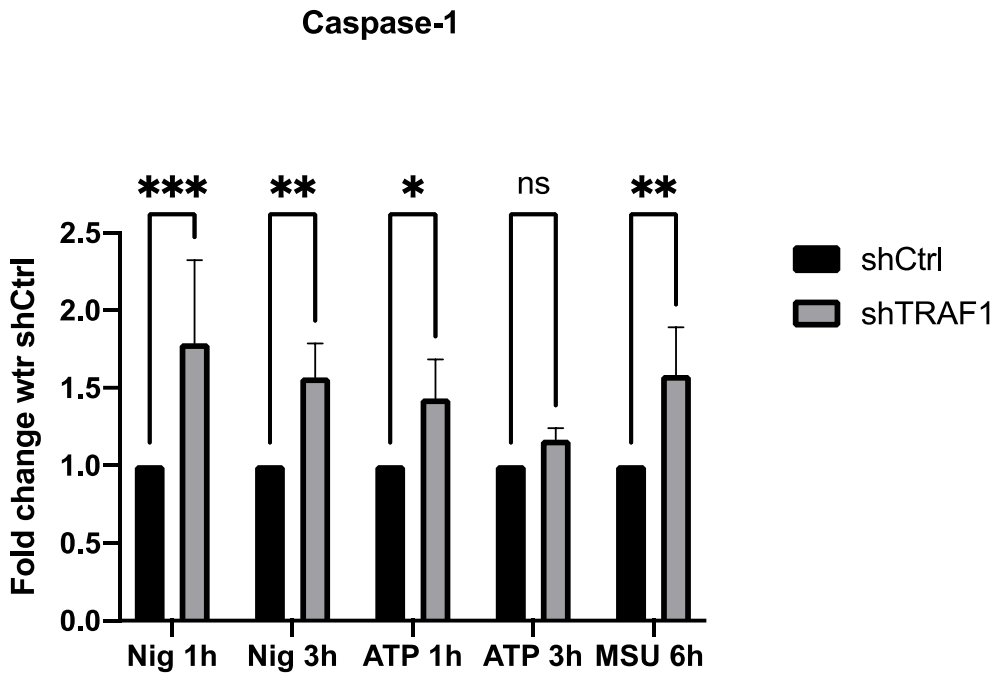

Figure 8. Fold change representation of caspase-1 activity in PMA-differentiated shControl and shTRAF1 THP-1 macrophages

Human monocytic shControl and shTRAF1 THP-1 cells were differentiated into macrophages using PMA (100 nM) overnight. The PMA induced macrophages were treated with LPS (100 ng/ml) for 3 hrs prior to stimulations with ATP (5 mM) and nigericin (10 uM) for 1 and 3 hrs. The PMA induced macrophages were treated with MSU (250 ug/ml) for 6 hrs. Culture supernatant was collected and analyzed for caspase-1 activity by Caspase-Glo® 1 Inflammasome Assay. The data represent fold change with respect to shControl. Values are means and standard deviations. The data shown are representative of four independent experiments. *=p< 0.05, **=p<0.01, ***=p<0.001 by two-way ANOVA.

4.6 Reduced TRAF1 Levels Lead to Increased ASC oligomerization

As discussed earlier, the oligomerization of ASC and formation of specks is an important step for NLRP3 inflammasome assembly and subsequent caspase-1 activation. Therefore, we investigated whether ASC oligomerization was regulated by TRAF1. The PMA-differentiated shControl and shTRAF1 were primed with LPS for 4 hrs (Signal 1) followed by ATP and nigericin stimulations of 30 min and 1h (Signal 2). Importantly, because ASC oligomerization is an upstream event, shorter stimulations time points were used. The data showed increased formation of ASC oligomers, dimers, and monomers upon stimulation with ATP and nigericin in

TRAF1 knockdown cells compared to control cells, which was essential to promote the activation of caspase-1 (Figure 9). Next, we sought to examine the mechanism by which TRAF1 regulates ASC oligomerization by looking at the linear ubiquitination of ASC.

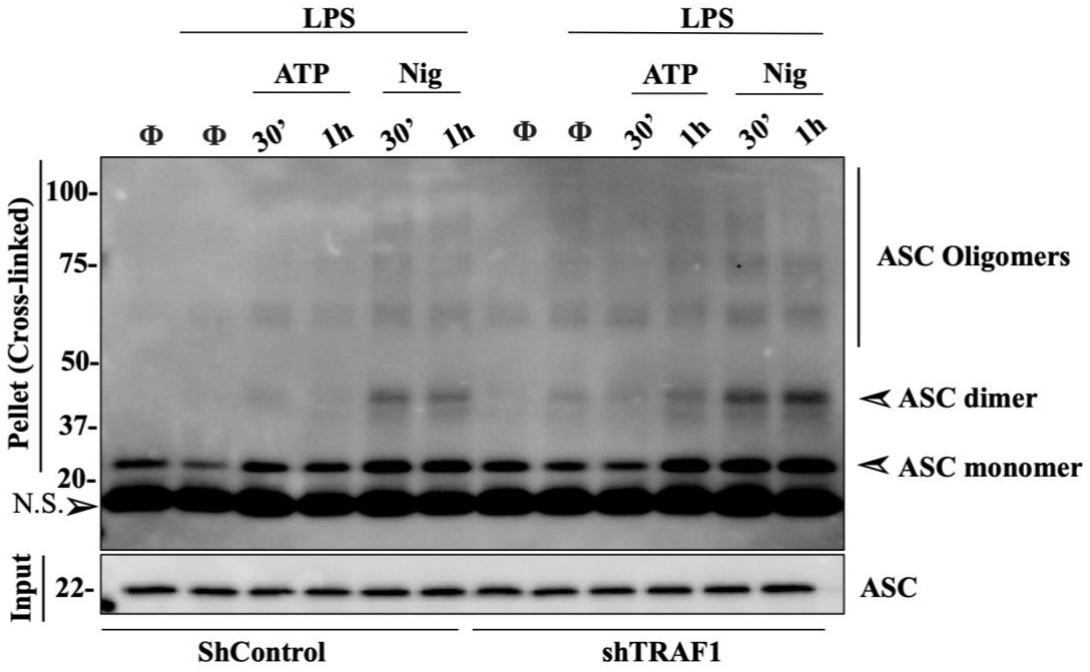

Figure 9. NLRP3 Inflammasome-dependent ASC oligomerization in PMA-differentiated shControl and shTRAF1 THP-1 macrophages

Human monocytic shControl and shTRAF1 THP-1 cells were differentiated into macrophages using PMA (100 nM) overnight. The PMA induced macrophages were treated with LPS 4 hrs (100 ng/ml) followed by ATP (5mM) and nigericin (10 uM) stimulations for 30' and 1 hr. Cells were lysed and the whole cell extract was obtained. Some of the lysates were kept as input and the rest were cross-linked with DSS. The crude pellets collected for the ASC oligomerization assay were resolved on a 13.5% gel and the input on a 10% gel. The samples and input were immunoblotted for ASC. N.S. represents non-specific binding due to immunoglobin heavy chain. The blot is representative of three independent experiments.

4.7 Reduced TRAF1 Levels Lead to Increased ASC Linear ubiquitination

To further examine the mechanism of TRAF1 regulation of NLRP3 inflammasome, we looked at the linear ubiquitination of ASC adaptor protein mediated by the LUBAC. As described previously, LUBAC consists of HOIL-1, HOIP, and SHARPIN, which acts as a regulator of NLRP3 inflammasome activation through linear ubiquitination of ASC. The PMA-differentiated shControl and shTRAF1 were primed with LPS followed by nigericin stimulation of 5, 15 ,30 min, and 1h. Next, immunoprecipitation of endogenous linear ubiquitin chains was performed using linear ubiquitin specific antibody that pulled down only linearly ubiquitinated ASC. Indeed, examining endogenous linear ubiquitination is notoriously difficult and other studies have utilized overexpression systems in 293T cells to study it (49). However, we opted to conduct the ubiquitination assay endogenously given the importance of this step and its physiological relevance. Strikingly, the results showed increased linear ubiquitination of ASC in shTRAF1 compared to shControl cells upon stimulations with nigericin (Figure 10). This signified the negative regulatory role of TRAF1 on LUBAC, which resulted in increased NLRP3 inflammasome activation as shown in the previous results.

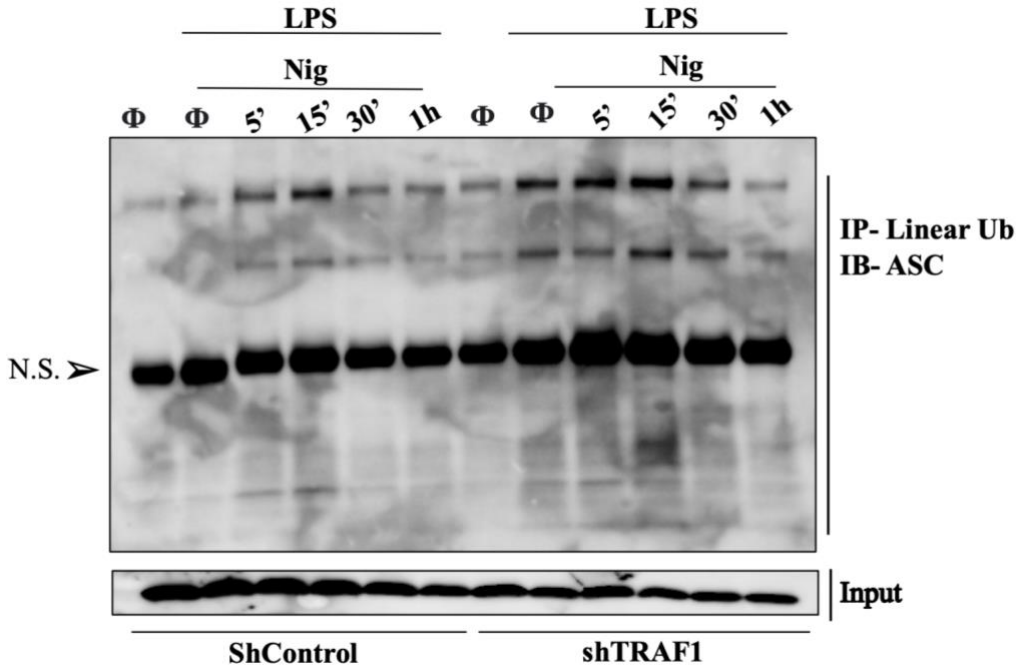

Figure 10. LUBAC-mediated ASC linear ubiquitination in PMA-differentiated shControl and shTRAF1 THP-1 macrophages

shControl and shTRAF1 THP-1 derived macrophages were primed with LPS 3h (100 ng/ml) and stimulated with nigericin for 5, 15, 30 min, and 1h. Cells were scraped and lysed to obtain the whole cell extracts. Immunoprecipitation of endogenous linear ubiquitin (IP-Linear Ub) chains was performed using linear ubiquitin specific antibody followed by immunoblotting for ASC. N.S. represents non-specific binding due to immunoglobin heavy chain. All blots are representative of three independent experiments.

4.8 Detection of Single Nucleotide Substitutions in TRAF1 Gene

4.8.1 Detecting Wild-Type and SNP Control Oligos

As described earlier, to examine the role of TRAF1 on NLRP3 inflammasome regulation independent its role on NF-κB regulation, we had to develop a model that allowed us to study TRAF1 in a context-dependent manner. Therefore, we aimed to create two versions of TRAF1 mutants from which one failed to interact with cIAP2, but maintained interaction with LUBAC (V203A), and other maintained interaction with cIAP2, yet failed to interact with LUBAC (S283A). Before creating the mutants (V203A & S283A) by employing CRISPR/Cas9, we had

to ensure that we had a functional assay to screen and detect the presence of the single-nucleotide substitutions in the TRAF1 gene. Therefore, we designed wild-type and knock-in mutants (V203A & S283) control oligos that encoded our desired target sequence, which served as positive controls in the screening process of the edited single-cell clones. To further confirm the functionality of our assay, we used two sets of controls provided in the screening kit that mimicked a mutant and a WT sequence. According to figure 11, the green and red fluorescence signals indicate the presence of mutant and WT sequences respectively. The strong green signal shows the presence of our desired mutation (V203A & S283A) in our designed mutant control oligos. Moreover, the strong red signals corresponded to a WT sequence of V203A and S283A that served to detect the non-edited sequences. The red fluorescent signal signified that cells had either chose non-homologous end joining (NHEJ) or had an unaltered genome. Lastly, the presence of both signals indicated a heterozygous containing both mutant and WT alleles. Therefore, this assay confirmed that all our mutations could be detected if they exist in the edited single-cell clones using CRISPR/Cas9 technique. Next, Cas9/sgRNA RNP complexes along with the donor single stranded DNA (ssDNA) were introduced into the THP-1 cells by electroporation and screened for presence of successful HDR events.

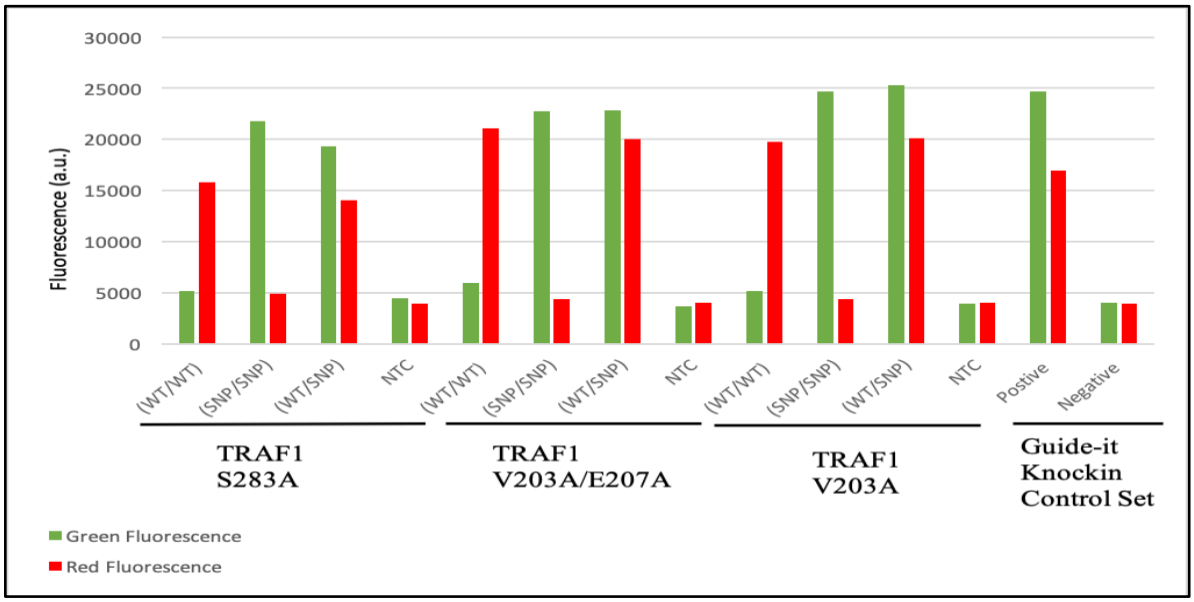

Figure 11. Optimized assay testing the functionality of displacement and flap-probe oligos designed to detect WT, heterozygous, and SNP in clones using designed control oligos

THP-1 genomic DNA was extracted and the region surrounding the target site was amplified using PCR. The PCR product was hybridized with the designed complementary displacement and flap-probe oligos. In case of a full hybridization between the amplified target site and the flap probe, the probe was cut by enzyme flapase and a green fluorescence was generated. In absence of complementary pairing, a red fluorescent signal was generated. The red and green fluorescent represent wild-type and SNP sequence respectively.

4.9 Genomic Cleavage of TRAF1 V203A site targeted by sgRNA in THP-1 Cells

Initially, we had to conduct a series of experiments in order to optimize several parameters that influenced the efficiency of our genome editing using CRISPR/Cas9 HDR system. These parameters included enhancing the electroporation efficiency for delivery of Cas9/sgRNA RNP complexes, optimizing the design of sgRNA and donor templates, and establishing an assay for detection of successful HDR events. After CRISPR/Cas9-mediated HDR was performed, we had to do single-cell cloning to isolate the genome-edited clones of interest among hundreds that were obtained. However, because the process of cloning is very labour intensive and time consuming, we first needed to check the functionality of our designed sgRNA and its ability to successfully target our locus of interest (V203A & S283A) in the TRAF1 gene before moving forward with isolating the single-cell clones. Thus, we examined the THP-1 bulk genome-edited population to ensure that our locus of interest was successfully targeted by the sgRNA. The guides were designed based on published algorithms that selected against off-target sites.

Followed CRISPR/Cas9-mediated HDR, the genomic DNA of THP-1 cells was extracted. Next, we designed primers to amplify the genomic indels that emerged as a result of electroporation at specific loci with double strand breaks using PCR. Afterwards, the PCR product was amplified and re-annealed followed by addition of a detection enzyme to detect the mismatches present in the genomic DNA. Also, we targeted the human AAVS1 gene that served as a positive control for the genomic DNA cleavage. As shown in Figure 12, the parental band for TRAF1 V203A is at 498 bp, which is cleaved into 190 bp and 308 bp. The presence of two fragments (190 bp and 308 bp) indicated successful TRAF1 V203A targeting by the sgRNA. On the other hand, the targeting of TRAF1 S283A locus was not successful as shown by a single

parental band at 466 bp. The result shows effective gene editing by V203A, but not S283A. Next, we proceeded to the second step, which was to identify HDR KI events (V203A) in the TRAF1 gene of the isolated clones.

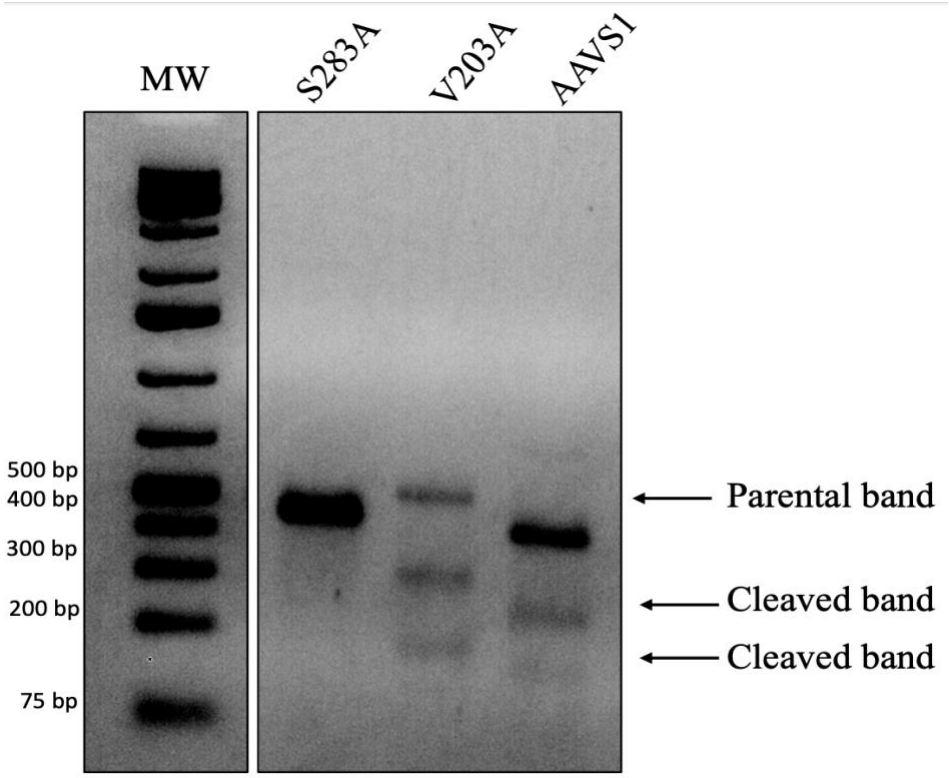

Figure 12. Gel image of CRISPR/Cas9-mediated cleavage in THP-1 cells
Gel image of genomic cleavage detection assay is shown for THP-1 cells. The samples were PCR amplified using S283A, V203A, and AAVS1 primers flanking the target site. After re-annealing, samples were treated with detection enzyme and DNA fragments were separated on a 2% agarose gel. Non-relevant samples were cut from the gel.

4.10 Screening for the Desired CRISPR/Cas9- mediated HDR KI V203A

The optimized assay described in section 4.8.1 was used to detect presence of any successful HDR KI events in the TRAF1 gene. Therefore, THP-1 single clones were screened for the presence of TRAF1 mutant V203A. We also included our designed control oligos of TRAF1 V203A mutant, heterozygous, and WT in the screening assay that served as an additional positive control for detection of successful HDR events. Analysis of 50 independent THP-1

clones from a total of 170 indicated presence of multiple candidates that had undergone HDR events. This was indicated by the presence of both green and red fluorescent signals that corresponded to a positive heterozygous clone with the desired mutation (V203A) (Figure 13). We were not able to detect any SNP in our clones due to the preference of DNA repair mechanisms for NHEJ rather than HDR. The next step was to send the clones for sequencing to confirm the gene sequence of the positive samples.

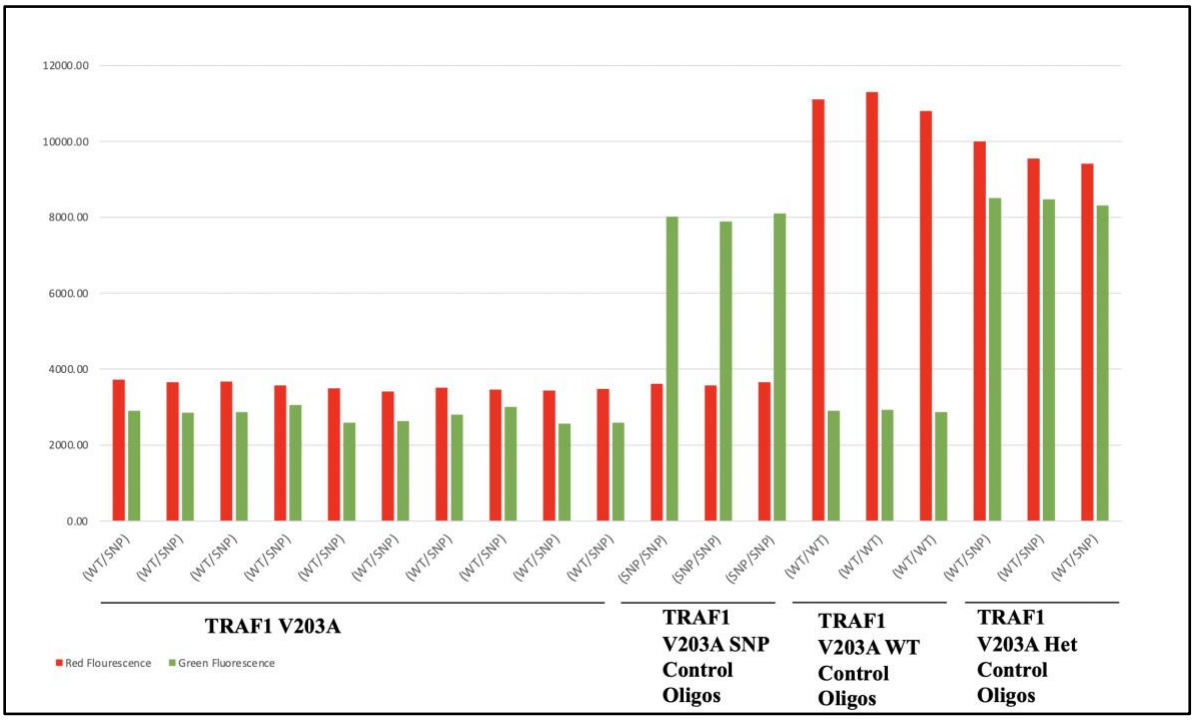

Figure 13. Screening THP-1 single-cell clones for detection of HDR events

Following CRISPR/Cas9 genome editing and clonal expansion, the genomic DNA of THP-1 clones was extracted. The region surrounding the target site was amplified using PCR. The PCR product was hybridized with the designed complementary displacement and flap-probe oligos. In case of a full hybridization between the amplified target site and the flap probe, the probe was cut by enzyme flapase and a green fluorescence signal was generated. In absence of complementary pairing, a red fluorescent signal was generated. The red and green fluorescent represent wild-type and SNP sequence respectively.

4.11 Sequencing Chromatographs for TRAF1 V203A Locus

After conducting CRISPR/Cas9 HDR, the genomic DNA of the selected clones was extracted, and the target region was PCR amplified. Then the PCR products were purified, and the DNA concentrations were measured. The quantity of the DNA was normalized between different samples and sent to sequencing for detection of SNPs in the TRAF1 gene at the V203A locus. As shown in Figure 14, the original TRAF1 V203 was a valine (GTC) that we aimed to mutate to alanine (GCC). The red and blue peaks denoted T and C nitrogenous bases respectively. The base substitution highlighted in blue exhibited the presence of a heterozygous edit identified by the overlapping peaks (blue and red) in the chromatograph. On the other hand, the presence of a single peak denoted the presence of WT TRAF1 with an unaltered sequence.

Ultimately, we obtained a heterozygous mutation at the V203A locus of the TRAF1 gene. Indeed, only three out of the fifty screened clones were heterozygous for the knock-in V203A. As expected, we predominantly found more NHEJ than HDR events due to the preference of the repair mechanism for NHEJ pathway than HDR pathway (65). Thus, as a by-product of HDR, we also obtained knock-ins with deletions or insertions that resulted in frameshift mutations and yielded TRAF1 knockout clones.

Figure 14. Sequencing chromatographs for TRAF1 mutant V203 KI in THP-1 cells

The genomic DNA of selected clones were extracted and purified, followed by PCR amplification of the target site and sequencing. Representative sequencing chromographs for wild-type and edited allele of TRAF1 gene are shown. Red and blue peaks denoted T and C bases respectively. The region with base substitution is highlighted in blue representing the heterozygous.

Chapter 5: Discussion

According to previous research, TRAF1 has been shown to play a role in inflammatory pathways including, TNFR and TLR by either promoting or limiting NF-κB activation. Abdul Sater et al. demonstrated that TRAF1 negatively regulates NF-κB activation by binding directly to components of LUBAC and thereby interfering with the linear ubiquitination of NEMO (60). Moreover, a study by Rodgers et al. showed that LUBAC is essential for NLRP3 inflammasome activation through regulation of ASC adaptor protein (49). As previously described, the NLRP3 inflammasome acts as a crucial component of innate immunity, yet its dysregulation has been implicated in an array of human auto-inflammatory and auto-immune diseases characterized by excessive IL-1β secretion (25, 26). Interestingly, around 20% of the population have an SNP in their TRAF1 gene associated with RA (61). Hence, understanding the underlying mechanism of TRAF1 regulation of NLRP3 activation is critical for developing therapies that allow for specific TRAF1 targeting to improve outcomes of NLRP3 inflammasome-related diseases. Thereby, we wanted to examine how TRAF1 might be regulating NLRP3 inflammasome activation mediated by LUBAC independently of its role in regulating NF-κB activation.

To elucidate the role of TRAF1 on NLRP3 inflammasome activation via LUBAC, we created a knockdown human monocytic THP-1 that had a low expression of TRAF1 protein. We used monocyte-derived macrophages as they are the first responders in case of an infection or damage, thus most applicable to this study. The PMA-differentiated macrophages shControl and shTRAF1 cells were treated with LPS that served as the first signal to increase the expression of NLRP3 and pro-IL-1β during the priming step through the NF-κB pathway. However, since a second signal was required for NLRP3 inflammasome activation, the cells were stimulated with extracellular ATP, nigericin, and MSU crystals. Our findings demonstrated the intracellular

molecular mechanism of NLRP3 inflammasome activation in the absence of TRAF1. We observed that upon stimulation with NLRP3 inflammasome inducers such as nigericin, ATP, and MSU, there was increased linear ubiquitination and oligomerization of ASC adaptor protein, which resulted in increased recruitment of active caspase-1 and mature IL-1β secretion. Given that LPS stimulation can also activate NF-κB pathway and lead to an increased expression of pro-inflammatory cytokines such as pro- IL-1β, we used MSU crystals as an additional inducer that does not require LPS priming step for promoting NLRP3 activation. Thus, demonstrating that MSU enhances NLRP3 inflammasome activation independent of IKK complex, which implies that downstream NF-κB signalling is not essential in promoting NLRP3 activation. Our results were consistent with a recent study that showed LUBAC linearly ubiquitinates ASC and enhances NLRP3 inflammasome activation in bone marrow macrophages independently of NF-κB activation (49). Therefore, in this study we showed that TRAF1 can play an important role in the regulation of NLRP3 inflammasome by limiting caspase-1 activation and IL-1β secretion via LUBAC, and act as a potential target for reducing the inflammatory response in autoinflammatory and autoimmune diseases such as RA.

Due to the multifaceted role of TRAF1 and its wide expression in various signalling pathways, it was important to develop a model to assess the role of TRAF1 in individual pathways. Work from our group had identified the site of interaction between TRAF1/cIAP2 (V203) downstream of TNFR and TRAF1/LUBAC (S283) downstream of TLR. Indeed, a single mutation of V203 to V203A, abrogated the interaction of TRAF1 with cIAP2, while allowed TRAF1 to maintain its interaction with LUBAC. On the other hand, a single mutation in S283 to S283A abrogated the interaction of TRAF1 with LUBAC without affecting the interaction with cIAP2 and associated signalling pathways. Hence, we employed CRISPR/Cas9 genome editing

method to create THP-1 cells with our desired mutations of V203A and S283A in the TRAF1 gene. The Cas9/sgRNA RNP complexes and donor ssDNA were introduced into THP-1 cells by electroporation and screened for the presence of a successful HDR KI (V203A and S283) events. We were able to obtain heterozygous mutations at the V203A locus of the TRAF1 gene and not the S283A. We had three heterozygous gene knock-in for TRAF1 mutant V203A among fifty clones that were screened. That is explained by the DNA repair mechanism preference for the process of NHEJ, which interferes with obtaining homozygous or heterozygous mutations through the HDR pathway. The rest of the TRAF1 V203A edited clones had used NHEJ-mediated deletion or insertion referred to as indels or remained unaltered WT. From the clones that contained indels, some were TRAF1 knockouts as the insertion or deletion resulted in a frameshift mutation and a subsequent stop codon.

Chapter 6: Future Directions

We were able to successfully create TRAF1 mutant V203A in THP-1 cells that fail to interact with cIAP2 but maintained interaction with the HOIL-1 subunit of LUBAC, and abrogated NF-κB activation. The next step would be to conduct experiments to look at the NLRP3 inflammasome activation, which should mimic a response similar to the TRAF1 knockdown cells. Moreover, to create the other TRAF1 mutant S283A that maintains interaction with cIAP2 and fails to bind to LUBAC by optimizing the design of sgRNA to target our locus of interest. Then conduct experiments to assess how the presence of TRAF1 would affect the inflammatory response through NLRP3 activation and processing of downstream products such as caspase-1 and IL-1β. This would be an additional way to examine the role of TRAF1 on NLRP3 inflammasome activation independent of its role on regulation of NF-κB activation downstream of TNFR.

With the insights of this study, we want to further examine the role of TRAF1 on the regulation of crystal-induced arthritis mediated by NLRP3 inflammasome in *vivo* by using mice that are WT, TRAF1$^{-/-}$, TRAF1^{LUBACmut}, and TRAF1^{cIAPmut}. As discussed before, deposition of MSU crystals in the joints acts as a danger signal activating the NLRP3 inflammasome to induce an inflammatory response. This results in an influx of neutrophils into the joint and release of active IL-1β. Thus, the mice will be injected with MSU crystals intra-articularly into the knee joints to induce gouty arthritis. The released IL-1β will be measured by ELISA and the neutrophils will be quantified using flow cytometry. Moreover, the knee joint swelling will be measured by a digital caliper. The findings from the in vivo studies will help to further examine the role of TRAF1 on NLRP3 inflammasome activation in relevant models of inflammatory diseases.

Chapter 7: References

1. Santoni, G., C. Cardinali, M. Morelli, M. Santoni, M. Nabissi, and C. Amantini. 2015. Danger- and pathogen-associated molecular patterns recognition by pattern-recognition receptors and ion channels of the transient receptor potential family triggers the inflammasome activation in immune cells and sensory neurons. *J. Neuroinflammation* 12: 21.
2. Tartey, S., and O. Takeuchi. 2017. Pathogen recognition and Toll-like receptor targeted therapeutics in innate immune cells. *Int. Rev. Immunol.* 36: 57–73.
3. Kelley, N., D. Jeltema, Y. Duan, and Y. He. 2019. The NLRP3 Inflammasome: An Overview of Mechanisms of Activation and Regulation. *Int. J. Mol. Sci.* 20: 3328.
4. Sahoo, B. R. 2020. Structure of fish Toll-like receptors (TLR) and NOD-like receptors (NLR). *Int. J. Biol. Macromol.* 161: 1602–1617.
5. Kufer, T. A., and P. J. Sansonetti. 2011. NLR functions beyond pathogen recognition. *Nat. Immunol.* 12: 121–128.
6. Piccinini, A. M., and K. S. Midwood. 2010. DAMPening Inflammation by Modulating TLR Signalling. *Mediators Inflamm.* 2010: 1–21.
7. Jin, J., Y. Xiao, H. Hu, Q. Zou, Y. Li, Y. Gao, W. Ge, X. Cheng, and S.-C. Sun. 2015. Proinflammatory TLR signalling is regulated by a TRAF2-dependent proteolysis mechanism in macrophages. *Nat. Commun.* 6: 5930.
8. Kumar, H., T. Kawai, and S. Akira. 2011. Pathogen Recognition by the Innate Immune System. *Int. Rev. Immunol.* 30: 16–34.
9. Dolasia, K., M. K. Bisht, G. Pradhan, A. Udgata, and S. Mukhopadhyay. 2018. TLRs/NLRs: Shaping the landscape of host immunity. *Int. Rev. Immunol.* 37: 3–19.
10. Uematsu, S., and S. Akira. 2006. Toll-like receptors and innate immunity. *J. Mol. Med.* 84: 712–725.
11. Verstrepen, L., T. Bekaert, T.-L. Chau, J. Tavernier, A. Chariot, and R. Beyaert. 2008. TLR-4, IL-1R and TNF-R signaling to NF-κB: variations on a common theme. *Cell. Mol. Life Sci.* 65: 2964–2978.
12. Kumar, V. 2020. Toll-like receptors in sepsis-associated cytokine storm and their endogenous negative regulators as future immunomodulatory targets. *Int. Immunopharmacol.* 89: 107087.
13. Fitzgerald, K. A., and J. C. Kagan. 2020. Toll-like Receptors and the Control of Immunity. *Cell* 180: 1044–1066.
14. Pourrajab, F., M. B. Yazdi, M. B. Zarch, M. B. Zarch, and S. Hekmatimoghaddam. 2015. Cross talk of the first-line defense TLRs with PI3K/Akt pathway, in preconditioning therapeutic approach. *Mol. Cell. Ther.* 3: 4.
15. Elinav, E., T. Strowig, J. Henao-Mejia, and R. A. Flavell. 2011. Regulation of the Antimicrobial Response by NLR Proteins. *Immunity* 34: 665–679.
16. Jin, C., and R. A. Flavell. 2010. Molecular Mechanism of NLRP3 Inflammasome Activation. *J. Clin. Immunol.* 30: 628–631.
17. He, Y., H. Hara, and G. Núñez. 2016. Mechanism and Regulation of NLRP3 Inflammasome Activation. *Trends Biochem. Sci.* 41: 1012–1021.
18. 2017. Inflammasomes in Myeloid Cells: Warriors Within. In *Myeloid Cells in Health and Disease* Gordon, ed. American Society of Microbiology. 305–324.
19. Lei-Leston, A. C., A. G. Murphy, and K. J. Maloy. 2017. Epithelial Cell Inflammasomes in Intestinal Immunity and Inflammation. *Front. Immunol.* 8: 1168.

20. Guo, H., J. B. Callaway, and J. P.-Y. Ting. 2015. Inflammasomes: mechanism of action, role in disease, and therapeutics. *Nat. Med.* 21: 677–687.
21. Proell, M., S. J. Riedl, J. H. Fritz, A. M. Rojas, and R. Schwarzenbacher. 2008. The Nod-Like Receptor (NLR) Family: A Tale of Similarities and Differences. *PLoS ONE* 3: e2119.
22. de Zoete, M. R., N. W. Palm, S. Zhu, and R. A. Flavell. 2014. Inflammasomes. *Cold Spring Harb. Perspect. Biol.* 6: a016287–a016287.
23. Gross, O., C. J. Thomas, G. Guarda, and J. Tschopp. 2011. The inflammasome: an integrated view: The inflammasome: an integrated view. *Immunol. Rev.* 243: 136–151.
24. Church, L. D., G. P. Cook, and M. F. McDermott. 2008. Primer: inflammasomes and interleukin 1β in inflammatory disorders. *Nat. Clin. Pract. Rheumatol.* 4: 34–42.
25. McAllister, M. J., M. Chemaly, A. J. Eakin, D. S. Gibson, and V. E. McGilligan. 2018. NLRP3 as a potentially novel biomarker for the management of osteoarthritis. *Osteoarthritis Cartilage* 26: 612–619.
26. Fusco, R., R. Siracusa, T. Genovese, S. Cuzzocrea, and R. Di Paola. 2020. Focus on the Role of NLRP3 Inflammasome in Diseases. *Int. J. Mol. Sci.* 21: 4223.
27. Yang, Q., R. Liu, Q. Yu, Y. Bi, and G. Liu. 2019. Metabolic regulation of inflammasomes in inflammation. *Immunology* 157: 95–109.
28. Kesavardhana, S., and T.-D. Kanneganti. 2017. Mechanisms governing inflammasome activation, assembly and pyroptosis induction. *Int. Immunol.* 29: 201–210.
29. Xue, Y., D. Enosi Tuipulotu, W. H. Tan, C. Kay, and S. M. Man. 2019. Emerging Activators and Regulators of Inflammasomes and Pyroptosis. *Trends Immunol.* 40: 1035–1052.
30. Szekanecz, Z., S. Szamosi, G. E. Kovács, E. Kocsis, and S. Benkő. 2019. The NLRP3 inflammasome - interleukin 1 pathway as a therapeutic target in gout. *Arch. Biochem. Biophys.* 670: 82–93.
31. Busso, N., and A. So. 2010. Mechanisms of inflammation in gout. 8.
32. Martinon, F., V. Pétrilli, A. Mayor, A. Tardivel, and J. Tschopp. 2006. Gout-associated uric acid crystals activate the NALP3 inflammasome. *Nature* 440: 237–241.
33. Choulaki, C., G. Papadaki, A. Repa, E. Kampouraki, K. Kambas, K. Ritis, G. Bertsias, D. T. Boumpas, and P. Sidiropoulos. 2015. Enhanced activity of NLRP3 inflammasome in peripheral blood cells of patients with active rheumatoid arthritis. *Arthritis Res. Ther.* 17: 257.
34. Guo, C., R. Fu, S. Wang, Y. Huang, X. Li, M. Zhou, J. Zhao, and N. Yang. 2018. NLRP3 inflammasome activation contributes to the pathogenesis of rheumatoid arthritis. *Clin. Exp. Immunol.* 194: 231–243.
35. Jo, E.-K., J. K. Kim, D.-M. Shin, and C. Sasakawa. 2016. Molecular mechanisms regulating NLRP3 inflammasome activation. *Cell. Mol. Immunol.* 13: 148–159.
36. Dick, M. S., L. Sborgi, S. Rühl, S. Hiller, and P. Broz. 2016. ASC filament formation serves as a signal amplification mechanism for inflammasomes. *Nat. Commun.* 7: 11929.
37. Huang, M. T.-H., D. J. Taxman, E. A. Holley-Guthrie, C. B. Moore, S. B. Willingham, V. Madden, R. K. Parsons, G. L. Featherstone, R. R. Arnold, B. P. O'Connor, and J. P.-Y. Ting. 2009. Critical Role of Apoptotic Speck Protein Containing a Caspase Recruitment Domain (ASC) and NLRP3 in Causing Necrosis and ASC Speck Formation Induced by *Porphyromonas gingivalis* in Human Cells. *J. Immunol.* 182: 2395–2404.
38. McKee, C. M., and R. C. Coll. 2020. NLRP3 inflammasome priming: A riddle wrapped in a mystery inside an enigma. *J. Leukoc. Biol.* 108: 937–952.
39. Groslambert, M., and B. Py. 2018. Spotlight on the NLRP3 inflammasome pathway. *J. Inflamm. Res.* Volume 11: 359–374.

40. Martinon, F. 2010. Signaling by ROS drives inflammasome activation. *Eur. J. Immunol.* 40: 616–619.
41. Sorbara, M. T., and S. E. Girardin. 2011. Mitochondrial ROS fuel the inflammasome. *Cell Res.* 21: 558–560.
42. Kubota, T., and R. Koike. 2010. Cryopyrin-associated periodic syndromes: background and therapeutics. *Mod. Rheumatol.* 20: 213–221.
43. Keddie, S., T. Parker, H. J. Lachmann, and L. Ginsberg. 2018. Cryopyrin-Associated Periodic Fever Syndrome and the Nervous System. *Curr. Treat. Options Neurol.* 20: 43.
44. de Torre-Minguela, C. 2017. The NLRP3 and Pyrin In ammasomes: Implications in the Pathophysiology of Autoin ammatory Diseases. *Front. Immunol.* 8: 17.
45. Hoseini, Z., F. Sepahvand, B. Rashidi, A. Sahebkar, A. Masoudifar, and H. Mirzaei. 2018. NLRP3 inflammasome: Its regulation and involvement in atherosclerosis. *J. Cell. Physiol.* 233: 2116–2132.
46. Lee, H.-M., J.-J. Kim, H. J. Kim, M. Shong, B. J. Ku, and E.-K. Jo. 2013. Upregulated NLRP3 Inflammasome Activation in Patients With Type 2 Diabetes. *Diabetes* 62: 194–204.
47. Song, N., and T. Li. 2018. Regulation of NLRP3 Inflammasome by Phosphorylation. *Front. Immunol.* 9: 2305.
48. Booshehri, L. M., and H. M. Hoffman. 2019. CAPS and NLRP3. *J. Clin. Immunol.* 39: 277–286.
49. Rodgers, M. A., J. W. Bowman, H. Fujita, N. Orazio, M. Shi, Q. Liang, R. Amatya, T. J. Kelly, K. Iwai, J. Ting, and J. U. Jung. 2014. The linear ubiquitin assembly complex (LUBAC) is essential for NLRP3 inflammasome activation. *J. Exp. Med.* 211: 1333–1347.
50. Bednash, J. S., and R. K. Mallampalli. 2016. Regulation of inflammasomes by ubiquitination. *Cell. Mol. Immunol.* 13: 722–728.
51. Gerlach, B., S. M. Cordier, A. C. Schmukle, C. H. Emmerich, E. Rieser, T. L. Haas, A. I. Webb, J. A. Rickard, H. Anderton, W. W.-L. Wong, U. Nachbur, L. Gangoda, U. Warnken, A. W. Purcell, J. Silke, and H. Walczak. 2011. Linear ubiquitination prevents inflammation and regulates immune signalling. *Nature* 471: 591–596.
52. Spit, M., E. Rieser, and H. Walczak. 2019. Linear ubiquitination at a glance. *J. Cell Sci.* 132: jcs208512.
53. Iwai, K. 2021. Discovery of linear ubiquitination, a crucial regulator for immune signaling and cell death. *FEBS J.* 288: 1060–1069.
54. Ohtake, F., and H. Tsuchiya. 2016. The emerging complexity of ubiquitin architecture. *J. Biochem. (Tokyo)* mvw088.
55. Emmerich, C. H., A. Ordureau, S. Strickson, J. S. C. Arthur, P. G. A. Pedrioli, D. Komander, and P. Cohen. 2013. Activation of the canonical IKK complex by K63/M1-linked hybrid ubiquitin chains. *Proc. Natl. Acad. Sci.* 110: 15247–15252.
56. Gurung, P., M. Lamkanfi, and T.-D. Kanneganti. 2015. Cutting Edge: SHARPIN Is Required for Optimal NLRP3 Inflammasome Activation. *J. Immunol.* 194: 2064–2067.
57. Tokunaga, F., S. Sakata, Y. Saeki, Y. Satomi, T. Kirisako, K. Kamei, T. Nakagawa, M. Kato, S. Murata, S. Yamaoka, M. Yamamoto, S. Akira, T. Takao, K. Tanaka, and K. Iwai. 2009. Involvement of linear polyubiquitylation of NEMO in NF-κB activation. *Nat. Cell Biol.* 11: 123–132.
58. Zapata, J. M., and J. C. Reed. TRAF1: Lord Without a RING. 6.
59. Xie, P. 2013. TRAF molecules in cell signaling and in human diseases. 31.

60. Abdul-Sater, A. A., M. I. Edilova, D. L. Clouthier, A. Mbanwi, E. Kremmer, and T. H. Watts. 2017. The signaling adaptor TRAF1 negatively regulates Toll-like receptor signaling and this underlies its role in rheumatic disease. *Nat. Immunol.* 18: 26–35.
61. Edilova, M. I., A. A. Abdul-Sater, and T. H. Watts. 2018. TRAF1 Signaling in Human Health and Disease. *Front. Immunol.* 9: 2969.
62. Tsitsikov, E. N., D. Laouini, I. F. Dunn, T. Y. Sannikova, L. Davidson, F. W. Alt, and R. S. Geha. TRAF1 Is a Negative Regulator of TNF Signaling: Enhanced TNF Signaling in TRAF1-Deficient Mice. 11.
63. Newton, K., M. L. Matsumoto, I. E. Wertz, D. S. Kirkpatrick, J. R. Lill, J. Tan, D. Dugger, N. Gordon, S. S. Sidhu, F. A. Fellouse, L. Komuves, D. M. French, R. E. Ferrando, C. Lam, D. Compaan, C. Yu, I. Bosanac, S. G. Hymowitz, R. F. Kelley, and V. M. Dixit. 2008. Ubiquitin Chain Editing Revealed by Polyubiquitin Linkage-Specific Antibodies. *Cell* 134: 668–678.
64. Matsumoto, M. L., K. C. Dong, C. Yu, L. Phu, X. Gao, R. N. Hannoush, S. G. Hymowitz, D. S. Kirkpatrick, V. M. Dixit, and R. F. Kelley. 2012. Engineering and Structural Characterization of a Linear Polyubiquitin-Specific Antibody. *J. Mol. Biol.* 418: 134–144.
65. Aumann, R. A., I. Häcker, and M. F. Schetelig. 2020. Female-to-male sex conversion in Ceratitis capitata by CRISPR/Cas9 HDR-induced point mutations in the sex determination gene transformer-2. *Sci. Rep.* 10: 18611.